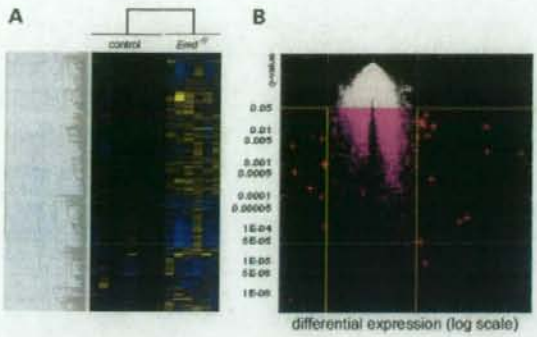

Figure 1. Affymetrix GeneChip expression profiling in hearts of *Emd*$^{-/y}$ mice. (**A**) Hierarchical clustering analysis of differentially expressed genes in hearts from control and *Emd*$^{-/y}$ mice. Rows indicate the expression of individual genes and vertical lines indicate each sample. For each gene, the ratio of transcript abundance in the samples to its abundance in the control is represented by color intensities (yellow indicates higher expression and blue indicates lower expression). (**B**) Volcano plots of absolute expression values ($\log_2$[q-value]) determined by robust multichip analysis. For each probe set, expression in hearts from *Emd*$^{-/y}$ mice is plotted. A two-fold threshold and $q < 0.05$ was used to determine the genes significantly altered in the analysis (yellow line squares).

Genes encoding myosin light chains (*Myl7*, 3.3 $\log_2$-fold; *Myl4*, 2.6 $\log_2$-fold) and myosin heavy chains (*Myh7*, 2.2 $\log_2$-fold) were upregulated. Similarly, there was upregulation of expression of genes encoding sarcolipin (*Sln*, 2.5 $\log_2$-fold), calcium channel L-type (*Cacna1C*, 1.2 $\log_2$-fold) and phospholamban (*Pln*, 1.1 $\log_2$-fold), proteins involved in cardiac contractility. The top-ranked genes identified in this analysis (*Myl4*, *Myl7*, *Myh7*, *Sln*) are common with those previously identified in hearts from *Lmna*$^{H222P/H222P}$ and *Lmna*$^{H222P/+}$ mice of the same age (33). Hence, upregulation of several identical gene signatures appears in hearts from animal models of both X-linked and autosomal dominant EDMD before any overt clinical or cardiac pathology.

To independently validate the expression of selected transcripts identified in the microarray analysis, we performed real-time quantitative RT–PCR using RNA extracted from hearts of mice different from those used for the microarrays. Primers corresponding to genes encoding myosin proteins (*Myl4*, *Myl7*, *Myh7*), polyadenylate binding protein-interacting protein 1 (*Paip1*), sarcolipin (*Sln*), peptidylglycine alpha-amidating monooxygenase (*Pam*), transferrin receptor (*Trfc*) and emerin (*Emd*) were selected as representative. Primers for *Emd* were chosen in the 3′ region following the portion of the gene containing the inserted neo^r cassette. For these genes, there was a strong correlation between real-time quantitative RT–PCR results and altered expression detected in the microarray analysis of hearts from *Emd*$^{-/y}$ mice (Fig. 2).

Functional class scoring analysis and ranked gene ontology classes

To obtain a global picture of the affected processes in hearts of *Emd*$^{-/y}$ mice, we used gene-class testing based on gene ontology (GO) terms. GO terms are functional categories that give information on the known biological processes associated with each gene. Because gene expression might be altered in related groups defined by pathways or functions rather than individually, genes showing coordinated but weak changes may be missed. We therefore used a semi-supervised method called functional class scoring, which examines the statistical distribution of individual gene expression scores among all genes in an ontology class. We can then identify GO terms with significant expression changes for which individual genes involved may not be identified as significant in single gene-profile analysis. Our functional class scoring analysis uses as input the 45 101 q-values from all the probes sets from the Affymetrix Mouse Genome 430 2.0 Arrays without an initial gene selection step. We used two different software packages, ermineJ and Ingenuity Pathway Analysis, which use different statistical approaches (see Materials and Methods).

Using ermineJ, we identified differential expression of GO classes involved in muscle contraction, transcription and translation, metabolism and angiogenesis in hearts from *Emd*$^{-/y}$ mice (Table 2). GO classes corresponding to signaling pathways were also affected in hearts of *Emd*$^{-/y}$ mice. These signaling pathways included JNK, MAPK, Wnt, I-kappaB kinase/NF-kappaB and TGF-β (Table 2). Most of the GO classes with altered expression in hearts of *Emd*$^{-/y}$ mice were previously identified in hearts of *Lmna*$^{H222P/H222P}$ (33). This suggested common molecular alterations downstream of *Lmna* and *Emd* mutations. Using Ingenuity Pathways Analysis, we identified the same pathways as with ermineJ in the *Emd*$^{-/y}$ mice. When Ingenuity Pathways Analysis was similarly used to analyze gene expression data from hearts of *Lmna*$^{H222P/H222P}$ mice (33), it identified genes of several similar pathways affected in hearts of *Emd*$^{-/y}$ mice (Fig. 3).

MAPK is activated in hearts of Emd knockout mice

Our analysis of functional classes of genes revealed significant differences in expression of the groups of genes encoding proteins of the MAPK pathway in hearts of *Emd*$^{-/y}$ mice. Because we previously identified activation of MAPK cascade in the *Lmna* H222P knock-in mouse model of autosomal dominant EDMD, we determined if it was similarly activated in hearts of the *Emd*$^{-/y}$ mouse model of X-linked EDMD. We evaluated the activation of two MAPKs, ERK1/2 and JNK, in hearts from control and *Emd*$^{-/y}$ mice. These kinases are activated by phosphorylation. Immunoblotting with antibody that recognized phosphorylated ERK1/2 demonstrated an increase in activated ERK1/2 in hearts from *Emd*$^{-/y}$ mice (Fig. 4A). However, using an antibody that recognized phosphorylated JNK, we did not detect an increase in activated JNK in hearts from *Emd*$^{-/y}$ mice (Fig. 4A). Phosphorylated ERK1/2 activates a series of downstream target genes, including those encoding elk-1 and atf-2. Immunoblotting with antibodies against elk-1 and atf-2 demonstrated increased expression of atf-2 but not elk-1 in hearts from *Emd*$^{-/y}$ mice compared to control mice (Fig. 4B). These data indicate an activation of ERK1/2 signaling in hearts from *Emd*$^{-/y}$ mice.

To compare the degree of ERK1/2 activation in hearts from *Emd*$^{-/y}$ and *Lmna*$^{H222P/H222P}$ mice, we measured the activated phosphorylated ERK1/2 by immunoblot. Phosphorylated

Table 1. Genes with altered expression as defined by $q < 0.05$ and ≥ 1 or ≤ -1 $\log_2$-fold change in hearts from *Emd*$^{-/y}$ mice

Probe set name	Gene symbol	Gene name	Log_2-fold	q-value
1449071_at	*Myl7*	Myosin, light polypeptide 7, regulatory	3.31	0.0020
1422580_at	*Myl4*	Myosin, light polypeptide 4, alkali; atrial, embryonic	2.55	0.0023
1420884_at	*Sln*	Sarcolipin	2.53	0.0128
1448553_at	*Myh7*	Myosin, heavy polypeptide 7, cardiac muscle, beta	2.12	2.15E-05
1425521_at	*Paip1*	Polyadenylate binding protein-interacting protein 1	1.94	1.62E-05
1454373_x_at	*Ubc*	Ubiquitin C	1.36	0.0132
1418908_at	*Pam*	Peptidylglycine alpha-amidating monooxygenase	1.31	0.0003
1435872_at	*Pim1*	Proviral integration site 1	1.23	0.0069
1420037_at	*Atp5a1*	ATP synthase, H+ transporting, mitochondrial F1 complex, alpha subunit, isoform 1	1.19	0.0294
1452661_at	*Tfrc*	Transferrin receptor	1.19	8.73E-07
1441679_at	*Cacna1c*	Calcium channel, voltage-dependent, L type, alpha 1C subunit	1.17	0.0136
1459238_at	*Pln*	Phospholamban	1.13	0.0163
1449824_at	*Prg4*	Proteoglycan 4 (megakaryocyte stimulating factor, articular superficial zone protein)	1.11	4.03E-06
1421534_at	*Fin15*	Fibroblast growth factor inducible 15	1.10	0.0189
1438714_at	*Zfp207*	Zinc finger protein 207	1.06	0.0146
1425099_a_at	*Arntl*	Aryl hydrocarbon receptor nuclear translocator-like	1.05	3.96E-06
1435602_at	*Sephs2*	Selenophosphate synthetase 2	1.05	0.0186
1432198_at	*6330414g02rik*	RIKEN cDNA 6330414G02 gene	1.02	0.0064
1456746_a_at	*Mic2l1*	MIC2 (monoclonal Imperial Cancer Research Fund 2)-like 1	−1.04	0.0009
1460434_at	*4833415n24rik*	RIKEN cDNA 4833415N24 gene	−1.06	1.14E-05
1416770_at	*Stk25*	Serine/threonine kinase 25 (yeast)	−1.08	0.0009
1449018_at	*Pfn1*	Profilin 1	−1.12	0.0056
1438009_at	*Hist1h2ae*	Histone 1, H2ae	−1.14	8.89E-05
1415997_at	*Txnip*	Thioredoxin interacting protein	−1.36	0.0064
1418174_at	*Dbp*	D site albumin promoter binding protein	−1.39	0.0002
1449526_a_at	*1110015e22rik*	RIKEN cDNA 1110015E22 gene	−1.80	0.0033
1417357_at	*Emd*	Emerin	−1.81	5.40E-08

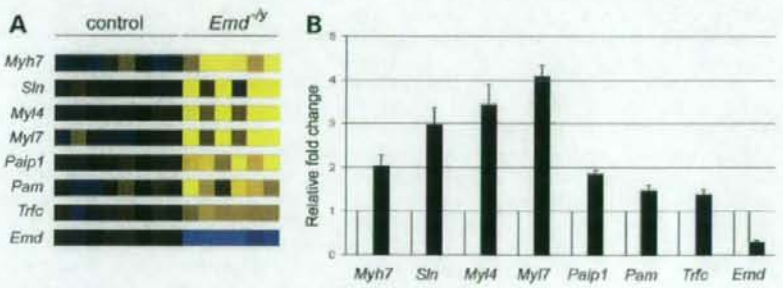

Figure 2. Validation of differential expression in hearts of *Emd*$^{-/y}$ mice of selected genes identified by GeneChips using real-time quantitative RT–PCR. (**A**) Matrices visualizing Affymetrix GeneChip data of corresponding probe sets of RNAs are shown at left of bar graph. In these matrices, each probe set is visualized as a row of colored squares with one square for each sample. (**B**) Bars indicate the fold overexpression of the indicated mRNA in hearts measured by real time quantitative RT–PCR as calculated by the $\Delta\Delta C_T$ method. White bars are values corresponding to the control mice and black bars are values corresponding to the *Emd*$^{-/y}$ mice. Values are means ± standard deviations for $n = 4$ samples per group. The real-time quantitative RT–PCR was performed in triplicate with the different RNA samples.

ERK1/2 was activated 2-fold in hearts from *Emd*$^{-/y}$ mice and 3-fold in hearts from *Lmna*$^{H222P/H222P}$ mice compared to hearts from control mice (Fig. 5). This showed a greater activation of ERK1/2 in hearts from *Lmna*$^{H222P/H222P}$ mice than in hearts from *Emd*$^{-/y}$ mice.

We analyzed the expression of additional genes normally activated downstream in the MAPK cascade using real-time quantitative RT–PCR. While these individual genes were not found to be significantly differentially expressed in our single gene-profile analysis, the fact that they are in MAPK GO classes suggested they may be activated. Expression of *c-jun* was statistically significantly increased in hearts from *Emd*$^{-/y}$ mice but expression of *Elk1* and *Elk4* was not (Fig. 6A). We further detected increases in expression of *Atf2*, *Atf4*, *Nfat2* and *Nfat4* in hearts from *Emd*$^{-/y}$ mice (Fig. 6A). To compare this model of X-linked EDMD to a model of autosomal dominant EDMD, we examined the expression of these same genes in hearts from *Lmna*$^{H222P/H222P}$ mice at 10 weeks of age. In hearts from these mice, there was significantly increased expression of all of these downstream factors

Table 2. Top-scoring GO terms listed with corresponding *P*-value and GO identification numbers in hearts from $Emd^{-/y}$ mice. The corresponding significant GO classes from $Lmna^{H222P/H222P}$ mice are reported

GO term	GO id	*P*-value	
		$Emd^{-/y}$	$Lmna^{H222P/H222P}$
Metabolism			
Coenzyme biosynthesis	GO:0009108	9.45E-11	3.97E-03
Phospholipid metabolism	GO:0006644	3.07E-10	7.68E-11
Sulfur metabolism	GO:0006790	1.23E-09	0.0342
Ribonucleotide metabolism	GO:0009259	5.34E-03	0.0204
C21-steroid hormone metabolism	GO:0006700	5.80E-03	0.0204
Organic acid biosynthesis	GO:0016053	6.83E-03	6.73E-03
Vitamin metabolism	GO:0006766	9.10E-03	0.0411
Tricarboxylic acid cycle	GO:0006099	9.83E-03	
Purine nucleotide metabolism	GO:0006163	0.0109	
Fatty acid biosynthesis	GO:0006633	0.0127	1.12E-10
Steroid biosynthesis	GO:0006694	0.0148	4.31E-03
Glycerophospholipid metabolism	GO:0006650	0.0211	
Gluconeogenesis	GO:0006094	0.0215	
Sphingolipid metabolism	GO:0006665	0.0249	4.55E-03
Sterol metabolism	GO:0016125	0.0294	0.0421
Pyruvate metabolism	GO:0006090	0.0310	
Cholesterol metabolism	GO:0008203	0.0316	0.0275
Nucleoside metabolism	GO:0009116	0.0362	
ATP metabolism	GO:0046034	0.0422	
Signaling pathways			
JNK cascade	GO:0007254	1.76E-10	5.12E-11
Rho protein signal transduction	GO:0007266	9.10E-03	
Wnt receptor signaling pathway	GO:0016055	9.22E-03	3.51E-11
Integrin-mediated signaling pathway	GO:0007229	0.0102	
Rac protein signal transduction	GO:0016601	0.0105	0.0116
Transmembrane receptor protein serine/threonine kinase signaling pathway	GO:0007178	0.0222	6.83E-11
I-kappaB kinase/NF-kappaB cascade	GO:0007249	0.0225	5.34E-03
Positive regulation of I-kappaB kinase/NF-kappaB cascade	GO:0043123	0.0310	9.06E-03
Positive regulation of JNK activity	GO:0043507	0.0319	4.39E-03
Activation of MAPK activity	GO:0000187	0.0354	6.30E-03
Transforming growth factor beta receptor signaling pathway	GO:0007179	0.0361	1.76E-10
Frizzled signaling pathway	GO:0007222	0.0483	0.0330
Transcription/translation			
Regulation of translation	GO:0006445	1.54E-10	
Chromatin remodeling	GO:0006338	0.0112	
DNA-dependent DNA replication	GO:0006261	0.0115	0.0111
Positive regulation of transcription, DNA-dependent	GO:0045893	0.0132	2.86E-11
MRNA polyadenylation	GO:0006378	0.0147	0.0271
Regulation of translational initiation	GO:0006446	0.0246	5.27E-03
MRNA 3'-end processing	GO:0031124	0.0262	
DNA methylation	GO:0006306	0.0287	
Muscle contraction			
Striated muscle contraction	GO:0006941	0.0134	3.07E-10
Angiogenesis			
Blood vessel development	GO:0001568	0.0120	2.46E-10
Angiogenesis	GO:0001525	0.0137	2.93E-11
Regulation of angiogenesis	GO:0045765	0.0320	0.0399

in the MAPK cascade (Fig. 6B). These results showed an activation of MAPK pathway in mouse models of X-linked and autosomal dominant EDMD; however, more downstream genes in MAPK pathway were activated in hearts from $Lmna^{H222P/H222P}$ mice.

To analyze *in vivo* activation of ERK1/2 in cardiac cells, we used an antibody that recognized phosphorylated ERK1/2 in sections of heart tissue. Histological examination of hearts revealed neither fibrosis nor inflammation or a significant number of cells other than cardiomyocytes (data not shown). Immunofluorescence microscopic labeling of heart sections from control mice with these antibodies revealed a rather diffuse fluorescence pattern, whereas fluorescence in hearts from $Emd^{-/y}$ mice was more intense and predominantly nuclear (Fig. 7A). Quantitative analysis of individual cardiomyocytes in the sections confirmed that the anti-phosphorylated ERK antibody labeled both cytoplasm and nucleus in hearts from control mice but essentially only the nucleus in hearts from $Emd^{-/y}$ mice (Fig. 7B). While fluorescence intensity of nuclear labeling was significantly higher in cardiomyocytes from $Emd^{-/y}$ mice compared to control mice, it was less than that in cardiomyocytes of

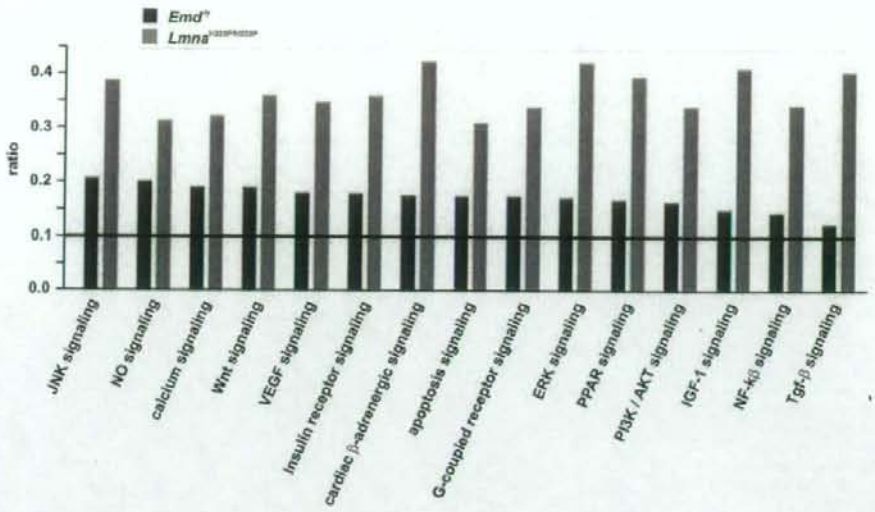

Figure 3. GO analysis of functional groups of genes differentially expressed in hearts of $Emd^{-/y}$ and $Lmna^{H222P/H222P}$ mice. The most significantly changed GO terms/pathways were identified by canonical pathways analysis using the Ingenuity Pathways Knowledge base. The ratio represents the number of genes from the data set that map to the pathway divided by the number of all known genes ascribed to the pathway.

$Lmna^{H222P/H222P}$ mice (Fig. 7C). These results suggested a gradient of activation and nuclear translocation of ERK1/2 in hearts from $Emd^{-/y}$ and $Lmna^{H222P/H222P}$ mice compared to control mice.

DISCUSSION

Although the causative genetic mutations have been identified and the descriptive pathology well documented, cellular mechanisms linking the genetic mutations to cardiac dysfunction in EDMD are unknown. We recently showed that in the *Lmna* H222P knock-in mouse model of autosomal dominant EDMD, there was activation of MAPK cascade and downstream targets in heart prior to the development of clinical or histological pathology (33). Genes encoding myosins and other sarcomeric proteins were also abnormally activated in these mice at an age when their hearts were histologically normal (33). In addition to being present in $Lmna^{H222P/H222P}$, which develop cardiomyopathy at approximately 8 weeks of age and have shortened life spans, similar early changes in gene expression were present in $Lmna^{H222P/+}$ mice, which do not develop significant cardiomyopathy and have normal life spans. In this study, we examined gene expression changes in the hearts of $Emd^{-/y}$ mice, a genetic model of X-linked EDMD. Similar to $Lmna^{H222P/+}$ mice, these mice apparently have normal life spans and do not develop clinically significant cardiomyopathy; however, they have small vacuoles mostly bordering nuclei in cardiomyocytes and develop mild first-degree heart block at 40 weeks of age (32). The $Emd^{-/y}$ mice had gene expression alterations in hearts similar to those in hearts of $Lmna^{H222P/+}$ and $Lmna^{H222P/H222P}$ mice, including activation of the ERK branch of the MAPK pathway.

It has been hypothesized that dilated cardiomyopathy-causing mutations affect force transmission from the sarcomere to the extra-sarcomeric cytoskeleton (36). In the present study, in which we performed genome-wide expression analysis in hearts from $Emd^{-/y}$ mice before any clinical cardiac abnormalities, we showed that genes encoding proteins involved in cardiac contraction are abnormally upregulated. The identified genes encoded either proteins of the sarcomere, such as β-myosin heavy chain and myosin light chain, or proteins involved in the Ca^{2+} homeostasis such as sarcolipin, calcium channel voltage-dependent L type and phospholamban. A concomitant deregulation of these two functional categories acting in muscle excitation-contraction is a common observation in cardiomyopathies (36,37).

We detected an abnormal activation of genes in the MAPK cascade in hearts of $Emd^{-/y}$ mice. For some of these genes, we found increased expression only by using real-time RT–PCR. Others and we have previously reported similar differences between microarrays and real-time RT–PCR for transcripts with a low absolute expression or when the difference of expression between the experimental and control are small (33,38,39). The fact that we also showed an increase in phosphorylation and nuclear translocation of ERK1/2 in cardiomyocytes strongly supports an activation of this branch of the MAPK cascade in hearts of $Emd^{-/y}$ mice. Although altered expression of the GO group defined as JNK cascade appeared significant in our statistical analysis using ermineJ and Ingenuity Systems, we did not detect activation of JNK in hearts of $Emd^{-/y}$ mice. This could be explained by the redundancy of functional classes in GO analysis. JNK and ERK1/2 are two branches of the MAPK pathway and have been described as activated by similar stimuli through the same G-protein-coupled receptors (40). Both kinases also acti-

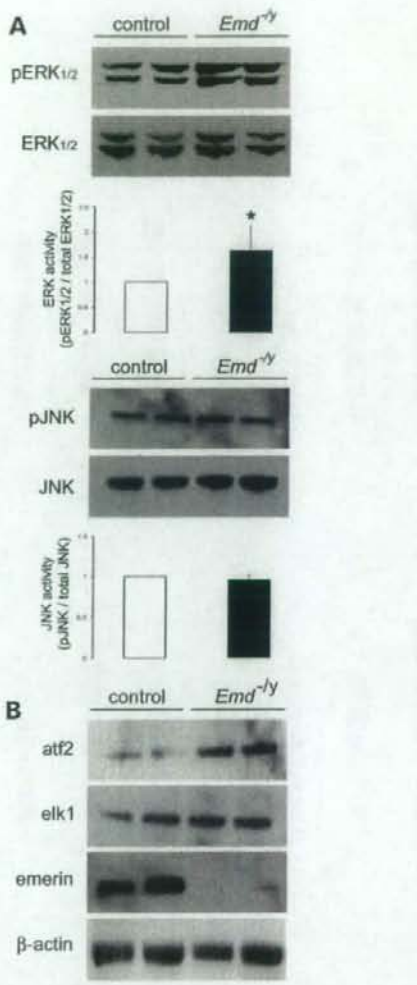

Figure 4. MAPK signaling is activated in hearts from $Emd^{-/y}$ mice. (**A**) Detection of phosphorylated ERK1/2 (pERK1/2), total ERK1/2, phosphorylated JNK (pJNK) and total ERK1/2 by immunoblotting of proteins extracted from hearts of control and $Emd^{-/y}$ mice. Data in bar graphs are means ± standard deviations for four samples per group (* $P < 0.05$). (**B**) Detection of elk-1, atf2 and emerin by immunoblotting of proteins extracted from hearts of control and $Emd^{-/y}$ mice. β-actin is used as an internal loading control.

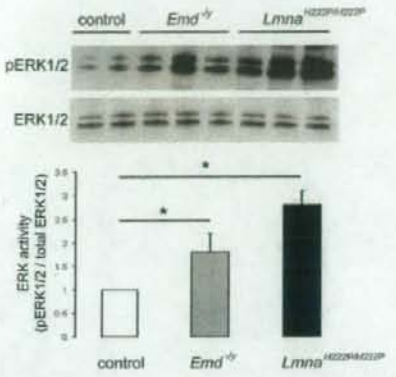

Figure 5. ERK1/2 activation in hearts from both $Emd^{-/y}$ and $Lmna^{H222P/H222P}$ mice. Detection of phosphorylated ERK1/2 (pERK1/2) and total ERK1/2 by immunoblotting of proteins extracted from hearts of control, $Emd^{-/y}$ and $Lmna^{H222P/H222P}$ mice. Data in bar graphs are means ± standard deviations (* $P < 0.05$).

vate the same downstream nuclear substrates (41). The dichotomy between the two branches is not entirely clear and is reflected by 55 probes sets corresponding to 22 genes in both the JNK and ERK1/2 GO functional classes.

Our results further showed that activation of MAPK cascade in hearts of $Emd^{-/y}$ mice was less significant than in hearts of $Lmna^{H222P/H222P}$ mice. We previously demonstrated that both ERK1/2 and JNK were activated in heart from $Lmna^{H222P/H222P}$ mice and to a lesser extent in hearts from $Lmna^{H222P/+}$ mice (33). In this study, we detected only an activation of ERK1/2 in hearts from $Emd^{-/y}$ mouse. We further showed that more downstream targets of MAPK were activated in hearts from $Lmna^{H222P/H222P}$ mice than in hearts from $Emd^{-/y}$ mice. The $Emd^{-/y}$ mice have slight cardiac dysfunction characterized by a mild prolongation of atrioventricular conduction time and vacuolization in cardiomyocytes (32). In contrast, male $Lmna^{H222P/H222P}$ mice develop cardiac chamber dilation associated with decreased left ventricle fractional shortening starting at 8 weeks of age (33). At 12 weeks of age, male $Lmna^{H222P/H222P}$ mice have pronounced conduction system abnormalities characterized by an increased atrioventricular conduction time. Male $Lmna^{H222P/H222P}$ mice die between 4 to 9 months of age. Two hypotheses can be raised to explain these differences between male $Lmna^{H222P/H222P}$ mice and $Emd^{-/y}$ mice. First, activation of the ERK branch of MAPK cascade may ultimately lead only to conduction defects in heart and not to pump failure. This hypothesis remains to be tested. Second, a relationship may exist between the degree of MAPK cascade activation and the severity of the heart disease. Our results suggest that this is more likely to be the case.

Several previous studies have implicated MAPK signaling in the development of cardiomyopathy. Overexpression of members of the ERK branch of MAPK cascade in mice causes cardiomyopathy (41–44). Activation of the MAPK cascade has also been reported in caveolin-3 (45), caveolin-1 (46) and p85 subunit of class I(A) PI3K (47) knockout mice, all of which develop cardiomyopathy. Activating mutations in *MEK1* and *MEK2* encoding kinases that activate ERK1 and ERK2 cause a cardio-facial-cutaneous syndrome (48). In addition, we previously demonstrated that the MAPK cascade is abnormally activated in hearts from *Lmna* H222P knock-in mice (33). The JNK branch of the MAPK cascade is also activated in dilated human hearts (49,50).

The results of this study and our previous work (33) suggest that activation of MAPK results directly from mutations in *Emd* and *Lmna* and that the MAPK activation

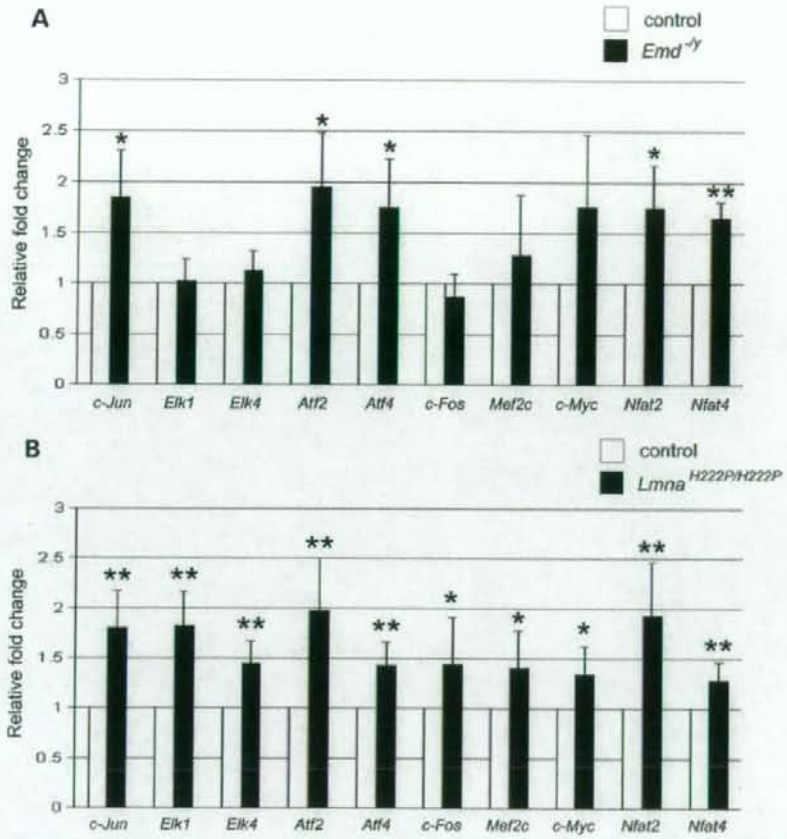

Figure 6. Expression of downstream genes in MAPK pathway in hearts from mouse models of EDMD. (**A**) Summary of real-time RT–PCR results in hearts from *Emd*$^{-/y}$ mice is shown. Bars indicate the fold overexpression of the indicated mRNA normalized to *Gapdh* as calculated by the $\Delta\Delta C_T$ method. Values are means ± standard deviations for $n = 4$ samples per group ($^*P < 0.05$). (**B**) Summary of real-time quantitative RT–PCR results in hearts from *Lmna*$^{H222P/H222P}$ mice is shown. Bars indicate the fold overexpression of the indicated mRNA normalized to *Gapdh* as calculated by the $\Delta\Delta C_T$ method. Values are means ± standard deviations for $n = 4$ samples per group ($^*P < 0.05$, $^{**}P < 0.005$).

leads to heart dysfunction. The mechanism of how mutations in genes encoding nuclear envelope proteins activate MAPK remains to be elucidated; however, ERK and JNK appear to be directly activated by the expression of A-type lamins with amino acid substitutions encoded by *LMNA* mutations that cause autsomal dominant EDMD (33). It remains to be determined if loss of emerin from cells similarly leads directly to MAPK cascade activation. Activation of MAPK leads to the further activation of several downstream target genes and we found several of these, including *c-Jun*, *Atf2*, *Atf4*, *Nfat2* and *Nfat4*, to be abnormally activated in hearts from *Emd*$^{-/y}$ and *Lmna* H222P mice. Transcription factors encoded by these genes can in turn regulate the expression of additional genes, including those encoding proteins involved in sarcomere structure, cardiomyofiber organization and other aspects of heart function (51,52). Abnormal expression of these proteins can lead to cardiomyopathy. Activation of the MAPK cascade has also been previously shown to regulate the calcium induced calcium-released mechanism, producing a negative inotropic effect (53,54). Hence, MAPK activation induced by abnormalities in emerin and A-type lamins can initiate a chain of events that leads to cardiomyopathy.

In summary, our data provide insights into the initial stages of cardiac pathology induced by defects in emerin and A-type lamins. Mutations in the genes encoding these proteins that cause EDMD lead to activation of MAPK signaling in hearts and changes in the expression of downstream genes implicated in the development of cardiomyopathy. These results have important practical implications because small molecule drugs can potentially be used to inhibit the different branches of the MAPK pathway (55,56).

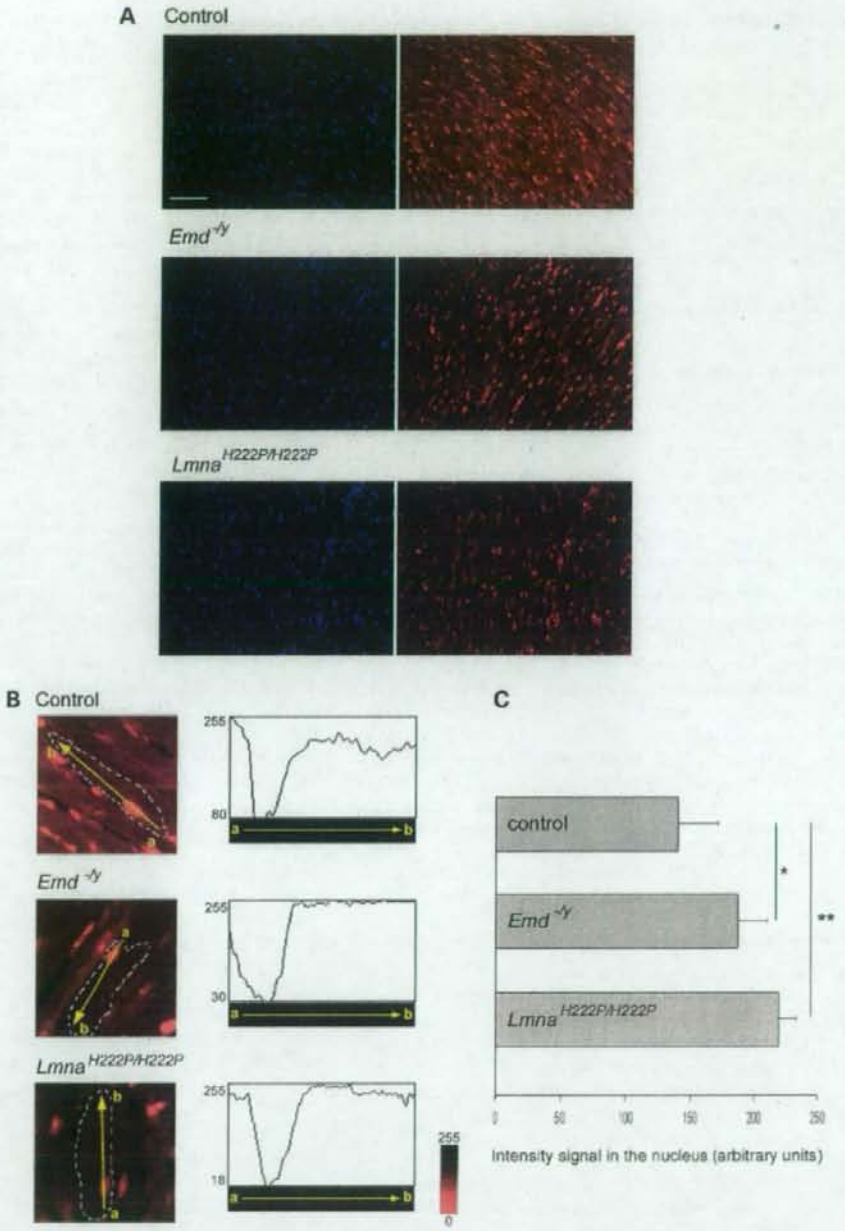

Figure 7. Immunofluorescence microscopic analysis of phopshorylated ERK1/2 (pERK) in heart sections from mouse models of EDMD. (**A**) Sections of frozen heart from control, *Emd* $^{-/y}$ and *Lmna* $^{H222P/H222P}$ mice were analyzed by immunofluorescence microscopy using anti-pERK1/2 antibody (red). Sections were counterstained with 4′,6-diamidino-2-phenylindole (blue). Bars: 50 μm. (**B**) Quantification of pERK1/2 labeling in cardiomyocytes from control, *Emd* $^{-/y}$ and *Lmna* $^{H222P/H222P}$ mice. Cardiomyocytes are delineated by dotted line and intensity of emitted fluorescence is measured along the yellow arrow (a to b). Intensity of the signal varies from 255 (absence of fluorescence) to 0 as reported on the scale; maximal intensity show on *y*-axis varies between panels. Position of the nucleus and intensity of fluorescence using mouse anti-pERK1/2 antibody is shown in the diagram of a single cardiomyocyte. (**C**) Quantification of pERK1/2 labeling in cardiomyocytes. Bars indicate intensity of pERK1/2 fluorescence in the nucleus of the indicated hearts. Values are means ± standard deviations for the intensity of nuclear fluorescence from $n = 80$ cardiomyocytes from two different hearts per group ($^{*}P < 0.05$, $^{**}P < 0.005$).

MATERIALS AND METHODS

Mice

Emd $^{-/y}$ mice (32) and *Lmna*$^{H222P/H222P}$ mice (28) were generated and genotyped as described.

RNA isolation

Total RNA was extracted from mouse hearts using the Rneasy isolation kit (Qiagen) according to the manufacturer's instructions. Adequacy and integrity of extracted RNA were determined by gel electrophoresis and concentrations measured by ultraviolet absorbance spectroscopy.

Microarray processing

We used Mouse Genome 430 2.0 GeneChip Arrays (Affymetrix). cDNA synthesis, cRNA synthesis and labeling were performed as described previously (33). Hybridization, washing, staining and scanning of arrays were performed at the Gene Chip Core Facility of the Columbia University Genome Center.

Microarray data analysis

Image files were obtained through Affymetrix GeneChip software and analyzed by robust multichip analysis using Affymetrix microarray '.cel' image file and GeneTraffic (Iobion Informatics) software. Robust multichip analysis is composed of three steps: background correction, quantile normalization and robust probe set summary. Genes were identified as differentially expressed if they met a false discovery rate threshold of 0.05 in a two-sample *t*-test (*q*-value) and showed at least a $\log_2$-fold difference in expression independent of absolute signal intensity. Our gene expression data are available in the National center for Biotechnology Information's Gene Expression Omnibus (GEO; http://www.ncbi.nlm.nih.gov/geo/), accessible through GEO Series accession number GSE6399.

Analysis of functional groups of genes

Gene expression changes related to functional groups were analyzed using the class score method in ermineJ (http://www.bioinformatics.ubc.ca/ermineJ/) (57) and the functional annotation method in Ingenuity Systems software (http://www.ingenuity.com). In ermineJ, the algorithm takes as input the log-transformed *t*-test *P*-values of genes that are members of a single GO class and estimates the probability that the set of *q*-values would occur by chance. Significant GO terms were identified using a false discovery rate of 0.05. In ingenuity systems, the identified canonical pathways were evaluated employing the right-tailed Fisher's exact test to calculate levels of significance. The *P*-value for each pathway was calculated by comparing the number of user-specified genes of interest that participated in a given function or pathway, relative to the total number of occurrences of these genes in all functional/pathway annotations stored in the ingenuity pathways knowledge base. Only annotations that have more Functions/Canonical Pathways Analysis genes than expected by chance ('right-tailed' annotations) were used.

Real-time RT–PCR analysis

Primers were designed correspond to mouse RNA sequences using Primer3 (http://frodo.wi.mit.edu/cgi-bin/primer3/primer3_www.cgi). RNA was extracted using Rneasy Protect Kit (Qiagen) and subsequently reverse transcribed using SuperScript first-strand synthesis system according to the manufacturer's instructions (Invitrogen). The real-time quantitative RT–PCR reaction contained iQ SYBR green super mix (Bio-Rad), 200 nM of primers and 0.2 µl of template in a 25 µl reaction volume. Amplification was carried out using the MyiQ Single-Color real-time PCR Detection System (Bio-Rad) with incubation times of 2 min at 95°C, followed by 50 cycles of 95°C for 30 s and 62°C for 30 s. Specificity of the amplification was checked by melting-curve analysis. Relative levels of mRNA expression were calculated according to the $\Delta\Delta C_T$ method, normalized by comparison to *Gapdh* mRNA expression.

Extraction of proteins from hearts and immunoblotting

Immunoblotting was performed as described previously (33). The following primary antibodies were used at dilutions from 1:200 to 1:1000: mouse monoclonal anti-emerin (Santa-Cruz), rabbit polyclonal anti-ERK1/2 (Santa-Cruz), rabbit polyclonal anti-pERK1/2 (Cell Signaling), rabbit polyclonal anti-JNK (Santa-Cruz), rabbit polyclonal anti-pJNK (Cell Signaling), anti-elk1 (Santa-Cruz), anti-atf-2 (Santa-Cruz) and anti-β-actin (Santa-Cruz). Secondary antibodies were HRP-conjugated (Amersham). Blots were developed using ECL (GE Healthcare) and exposed to X-OMAT film (Kodak) for appropriate periods of time. Band densities were calculated using Scion Image software (Scion Corporation) and normalized to the appropriate total JNK or ERK1/2 of protein extracts.

Immunofluorescence microscopy

For immunohistochemistry, 8 µm frozen sections of transversal cardiac muscles were fixed in 3.7% formaldehyde in phosphate-buffered saline for 15 min and then blocked in 5% fetal goat serum in phosphate-buffered saline containing 0.5% Triton X-100 for 1 h. Antibodies used were primary mouse anti-pERK1/2 (Cell Signaling) and secondary Texas Red conjugated anti-mouse (Molecular Probes). Sections were counterstained with 0.1 µg/ml 4′,6-diamidino-2-phenylindole (Sigma-Aldrich). Specimens were observed using a Microphot SA (Nikon). Images were collected using a Spot RT Slide camera (Diagnostic Instruments) linked to a PC computer running Adobe Photoshop 6.0 (Adobe Systems). Fluorescence intensity in cardiomyocytes was measured using Scion Image software (Scion Corporation). Data are reported as means ± standard deviations and are compared with respective controls using a two-tailed *t*-test.

ACKNOWLEDGEMENTS

We thank T. Arimura and V. Decostre for assistance with breeding and analyzing *Lmna* H222P mice, A. Gharavi for assistance with real-time quantitative RT PCR, V. Miljkovic for assistance with hybridization of Affymetrix GeneChips

and J. Ribeiro, C. Derognat and S. Mafray for helpful discussions. A.M. was supported in part by fellowship grants from Association Française contre les Myopathies and Fondation pour la Recherche Médicale. This work was supported primarily by a grant from the National Institutes of Health (AR048997) to H.J.W. It was also supported by grants for Research on Psychiatric and Neurological Diseases and Mental Health from Health and Labor Sciences Research, Scientific Research from the Japan Society for the Promotion of Science and the Nervous and Mental Disorders and from the Japan Ministry of Health, Labor and Welfare to Y.K.H.; from the Human Frontiers Science Program (RGP0057/2001-M) to H.J.W., Y.K.H. and G.B.; and from the European Union Sixth Framework (Euro-laminopathies, Contract No. 018690) and from Association Française contre les Myopathies (No. 11057) to G.B.

Conflict of Interest statement. None declared.

REFERENCES

1. Emery, A.E.H. (2000) Emery–Dreifuss muscular dystrophy—a 40 year retrospective. *Neuromusc. Disord.*, **10**, 228–232.
2. Bione, S., Maestrini, E., Rivella, S., Mancini, M., Regis, S., Romeo, G. and Toniolo, D. (1994) Identification of a novel X-linked gene responsible for Emery–Dreifuss muscular dystrophy. *Nat. Genet.*, **8**, 323–327.
3. Nagano, A., Koga, R., Ogawa, M., Kurano, Y., Kawada, J., Okada, R., Hayashi, Y.K., Tsukahara, T. and Arahata, K. (1996) Emerin deficiency at the nuclear membrane in patients with Emery–Dreifuss muscular dystrophy. *Nat. Genet.*, **12**, 254–259.
4. Manilal, S., Nguyen, T.M., Sewry, C.A. and Morris, G.E. (1996) The Emery–Dreifuss muscular dystrophy protein, emerin, is a nuclear membrane. *Hum. Mol. Genet.*, **5**, 801–808.
5. Cartegni, L., Di Barletta, M.R., Barresi, R., Squarzoni, S., Sabatelli, P., Maraldi, N., Mora, M., Di Blasi, C., Comelio, F., Merlini, L. *et al.* (1997) Heart specific localization of emerin: new insights into Emery–Dreifuss muscular dystrophy. *Hum. Mol. Genet.*, **6**, 2257–2264.
6. Bengtsson, L. and Wilson, K.L. (2004) Multiple and surprising new functions for emerin, a nuclear membrane protein. *Curr. Opin. Cell Biol.*, **16**, 73–79.
7. Markiewicz, E., Tilgner, K., Barker, N., van de Wetering, M., Clevers, H., Dorobek, M., Hausmanowa-Petrusewicz, I., Ramaekers, F.C.S., Broers, J.L.V., Blankesteijn, W.M. *et al.* (2006) The inner nuclear membrane protein emerin regulates β-catenin activity by restricting its accumulation in the nucleus. *EMBO J.*, **25**, 3275–3285.
8. Bonne, G., Di Barletta, M.R., Varnous, S., Becane, H.M., Hammouda, E.H., Merlini, L., Muntoni, F., Greenberg, C.R., Gary, F., Urtizberea, J.A. *et al.* (1999) Mutations in the gene encoding lamin A/C cause autosomal dominant Emery–Dreifuss muscular dystrophy. *Nat. Genet.*, **21**, 285–288.
9. Lin, F. and Worman, H.J. (1993) Structural organization of the human gene encoding nuclear lamin A and nuclear lamin C. *J. Biol. Chem.*, **268**, 16321–16326.
10. McKeon, F.D., Kirschner, M.W. and Caput, D. (1986) Homologies in both primary and secondary structure between nuclear envelope and intermediate filament proteins. *Nature*, **319**, 463–468.
11. Fisher, D.Z., Chaudhary, N. and Blobel, G. (1986) cDNA sequencing of nuclear lamins A and C reveals primary and secondary structural homology to intermediate filament proteins. *Proc. Natl Acad. Sci. USA*, **83**, 6450–6454.
12. Aebi, U., Cohn, J., Buhle, L. and Gerace, L. (1986) The nuclear lamina is a meshwork of intermediate-type filaments. *Nature*, **323**, 560–564.
13. Goldman, A.E., Maul, G., Steinert, P.M., Yang, H.Y. and Goldman, R.D. (1986) Keratin-like proteins that co-isolate with intermediate filaments of BHK-21 cells are nuclear lamins. *Proc. Natl Acad. Sci. USA*, **83**, 3839–3843.
14. Liu, J., Rolef Ben-Shahar, T., Riemer, D., Treinin, M., Spann, P., Weber, K., Fire, A. and Gruenbaum, Y. (2000) Essential roles for *Caenorhabditis elegans* lamin gene in nuclear organization, cell cycle progression, and spatial organization of nuclear pore complexes. *Mol. Biol. Cell.*, **11**, 3937–3947.
15. Muchir, A., van Engelen, B.G., Lammens, M., Mislow, J.M., McNally, E., Schwartz, K. and Bonne, G. (2003) Nuclear envelope alterations in fibroblasts from LGMD1B patients carrying nonsense Y259X heterozygous or homozygous mutation in lamin A/C gene. *Exp. Cell. Res.*, **291**, 352–362.
16. Muchir, A., Medioni, J., Laluc, M., Massart, C., Arimura, T., van Der Kooi, A.J., Desguerre, I., Mayer, M., Ferrer, X., Briault, S. *et al.* (2004) Nuclear envelope alterations in fibroblasts from patients with muscular dystrophy, cardiomyopathy and partial lipodystrophy carrying lamin A/C gene mutations. *Muscle Nerve*, **30**, 444–450.
17. Vigouroux, C., Auclair, M., Dubosclard, E., Pouchelet, M., Capeau, J., Courvalinn, J.C. and Buendia, B. (2001) Nuclear envelope disorganization in fibroblasts from lipodystrophic patients with heterozygous R482Q/W mutations in lamin A/C gene. *J. Cell Sci.*, **114**, 4459–4468.
18. Worman, H.J. and Gundersen, G.G. (2006) Here come the SUNs: a nucleocytoskeletal missing link. *Trends Cell Biol.*, **16**, 67–69.
19. Spann, T.P., Moir, R.D., Goldman, A.E., Stick, R. and Goldman, R.D. (1997) Disruption of nuclear lamin organization alters the distribution of replication factors and inhibits DNA synthesis. *J. Cell Biol.*, **136**, 1201–1212.
20. Moir, R.D., Spann, T.P., Herrmann, H. and Goldman, R.D. (2000) Disruption of nuclear lamin organization blocks the elongation phase of DNA replication. *J. Cell Biol.*, **149**, 1179–1192.
21. Spann, T.P., Goldman, A.E., Wang, C., Huang, S. and Goldman, R.D. (2002) Alteration of nuclear lamin organization inhibits RNA polymerase II-dependent transcription. *J. Cell Biol.*, **156**, 603–608.
22. Worman, H.J. and Courvalin, J.C. (2000) The inner nuclear membrane. *J. Membr. Biol.*, **177**, 1–11.
23. Fairley, E.A., Kendrick-Jones, J. and Ellis, J.A. (1999) The Emery–Dreifuss muscular dystrophy phenotype arises from aberrant targeting and binding of emerin at the inner nuclear membrane. *J. Cell Sci.*, **112**, 2571–2582.
24. Clements, L., Manilal, S., Love, D.R. and Morris, G.E. (2000) Direct interaction between emerin and lamin A. *Biochem. Biophys. Res. Commun.*, **267**, 709–714.
25. Sakaki, M., Koike, H., Takahashi, N., Sasagawa, N., Tomioka, S., Arahata, K. and Ishiura, S. (2001) Interaction between emerin and nuclear lamins. *J. Biochem.*, **129**, 321–327.
26. Muchir, A. and Worman, H.J. (2004) The nuclear envelope and human disease. *Physiology*, **19**, 309–314.
27. Sullivan, T., Escalante-Alcalde, D., Bhatt, H., Anver, M., Bhat, N., Nagashima, K., Stewart, C.L. and Burke, B. (1999) Loss of A-type lamin expression compromises nuclear envelope integrity leading to muscular dystrophy. *J. Cell Biol.*, **147**, 913–920.
28. Arimura, T., Helbling-Leclerc, A., Massart, C., Varnous, S., Niel, F., Lacène, F., Fromes, Y., Toussaint, M., Mura, A-M., Keller, D.I. *et al.* (2005) Mouse model carrying H222P-*Lmna* mutation develops muscular dystrophy and dilated cardiomyopathy similar to human striated muscle laminopathies. *Hum. Mol. Genet.*, **14**, 155–169.
29. Mounkes, L.C., Kozlov, S.V., Rottman, J.N. and Stewart, C.L. (2005) Expression of an *LMNA*-N195K variant of A-type lamins results in cardiac conduction defects and death in mice. *Hum. Mol. Genet.*, **14**, 2167–2180.
30. Wang, Y., Herron, A.J. and Worman, H.J. (2006) Pathology and nuclear abnormalities in hearts of transgenic mice expressing M371K lamin A encoded by an *LMNA* mutation causing Emery–Dreifuss muscular dystrophy. *Hum. Mol. Genet.*, **15**, 2479–2489.
31. Meleon, G., Kozlov, S., Cutler, D.A., Sullivan, T., Hernandez, L., Zhao, P., Mitchell, S., Nader, G., Bakay, M., Rottman, J.N. *et al.* (2006) Loss of emerin at the nuclear envelope disrupts the Rb1/E2F and MyoD pathways during muscle regeneration. *Hum. Mol. Genet.*, **15**, 637–651.
32. Ozawa, R., Hayashi, Y.K., Ogawa, M., Kurokawa, R., Matsumoto, H., Noguchi, S., Nonaka, I. and Nishino, I. (2006) Emerin-lacking mice show minimal motor and cardiac dysfunctions with nuclear-associated vacuoles. *Am. J. Pathol.*, **168**, 907–917.
33. Muchir, A., Pavlidis, P., Decostre, V., Herron, A.J., Arimura, T., Bonne, G. and Worman, H.J. (2007) Activation of MAPK pathway links *LMNA* mutations to cardiomyopathy in Emery–Dreifuss muscular dystrophy. *J. Clin. Invest.*, **117**, 1282–1293.

34. Petrich, B.G., Gong, X., Lerner, D.L., Wang, X., Brown, J.H., Saffitz, J.E. and Wang, Y. (2002) c-Jun N-terminal kinase activation mediates downregulation of connexin43 in cardiomyocytes. *Circ. Res.*, **91**, 640–647.
35. Petrich, B.G., Molkentin, J.D. and Wang, Y. (2003) Temporal activation of c-Jun N-terminal kinase in adult transgenic heart via cre-loxP-mediated DNA recombination. *FASEB J.*, **17**, 749–751.
36. Morita, H., Seidman, J. and Seidman, C.E. (2005) Genetic causes of human heart failure. *J. Clin. Invest.*, **115**, 518–526.
37. Yano, M., Ikeda, Y. and Matsuzaki, M. (2005) Altered intracellular Ca2+ handling in heart failure. *J. Clin. Invest.*, **115**, 556–564.
38. Qin, L.X., Beyer, R.P., Hudson, F.N., Linford, N.J., Morris, D.E. and Kerr, K.F. (2006) Evaluation of methods for oligonucleoyides array data via quantitative real time PCR. *BMC Bioinformatics*, **7**, 23.
39. Millenaar, F.F., Okyere, J., May, S.T., van Zanten, M., Voesenek, L.A. and Peeters, A.J. (2006) How to decide? Different methods of calculating gene expression from short oligonucleotide array data will give different results. *BMC Bioinformatics*, **7**, 137.
40. Michel, M.C., Li, Y. and Heusch, G. (2001) Mitogen-activated protein kinases in the heart. *Naunyn Schmiedebergs Arch. Pharmacol.*, **363**, 245–266.
41. Liang, Q. and Molkentin, J.D. (2003) Redefining the roles of p38 and JNK signaling in cardiac hypertrophy: dichotomy between cultured myocytes and animals models. *J. Mol. Cell. Cardiol*, **35**, 1385–1394.
42. Braz, J.C., Bueno, O.F., Liang, Q., Wilkins, B.J., Dai, Y.S., Parsons, S., Braunwart, J., Glascock, B.J., Klevitsky, R., Kimball, T.F. *et al.* (2003) Targeted inhibition of p38 MAPK promotes hypertrophic cardiomyopathy through upregulation of calcineurin-NFAT signaling. *J. Clin. Invest.*, **111**, 1475–1486.
43. Nicol, R.L., Frey, N., Pearson, G., Cobb, M., Richardson, J. and Olson, E.N. (2001) Activated MEK5 induces serial assembly of sarcomeres and eccentric cardiac hypertrophy. *EMBO J.*, **20**, 2757–2767.
44. Bueno, O.F., De Windt, L.J., Tymitz, K.M., Witt, S.A., Kimball, T.R., Klevitsky, R., Hewett, T.E., Jones, S.P., Lefer, D.J., Peng, C.F. *et al.* (2000) The MEK1-ERK1/2 signaling pathway promotes compensated cardiac hypertrophy in transgenic mice. *EMBO J.*, **19**, 6341–6350.
45. Woodman, S.E., Park, D.S., Cohen, A.W., Cheung, M.W., Chandra, M., Shirani, J., Tang, B., Jelicks, L.A., Kitsis, R.N., Christ, G.J. *et al.* (2002) Caveolin-3 knock-out mice develop a progressive cardiomyopathy and show hyperactivation of the p42/44 MAPK cascade. *J. Biol. Chem.*, **277**, 38988–38997.
46. Cohen, A.W., Park, D.S., Woodman, S.E., Williams, T.M., Chandra, M., Shirani, J., Pereira de Souza, A., Kitsis, R.N., Russell, R.G., Weiss, L.M. *et al.* (2003) Caveolin-1 null mice develop cardiac hypertrophy with hyperactivation of p42/44 MAP kinase in cardiac fibroblasts. *Am. J. Physiol. Cell. Physiol.*, **284**, 457–474.
47. Luo, J., McMullen, J.R., Sobkiw, C.L., Zhang, L., Dorfman, A.L., Sherwood, M.C., Logsdon, M.N., Horner, J.W., DePinho, R.A., Izumo, S. *et al.* (2005) Class IA phosphoinositide 3-kinase regulates heart size and physiological cardiac hypertrophy. *Mol. Cell. Biol.*, **25**, 9491–9502.
48. Rodriguez-Viciana, P., Tetsu, O., Tidyman, W.E., Estep, A.L., Conger, B.A., Santa Cruz, M., McCormick, F. and Rauen, K.A. (2006) Germline mutations in genes within the MAPK pathway cause cardio-facio-cutaneous syndrome. *Science*, **311**, 1287–1290.
49. Cook, S.A., Sugden, P.H. and Clerk, A. (1999) Activation of c-Jun N-terminal kinases and p38-mitogen-activated protein kinases in human heart failure secondary to ischaemic heart disease. *J. Mol. Cell. Cardiol.*, **31**, 1429–1434.
50. Haq, S., Choukroun, G., Lim, H., Tymitz, K.M., del Monte, F., Gwathmey, J., Grazette, L., Michael, A., Hajjar, R., Force, T. *et al.* (2001) Differential activation of signal transduction pathways in human hearts with hypertrophy versus advanced heart failure. *Circulation*, **103**, 670–677.
51. Gillespie-Brown, J., Fuller, S.J., Bogoyevitch, M.A., Cowley, S. and Sugden, P.H. (1995) The mitogen-activated protein kinase kinase MEK1 stimulates a pattern of gene expression typical of the hypertrophic phenotype in rat ventricular cardiomyocytes. *J. Biol. Chem.*, **270**, 28092–28096.
52. Thorburn, J., Carlson, M., Mansour, S.J., Chien, K.R., Ahn, N.G. and Thorburn, A. (1995) Inhibition of a signaling pathway in cardiac muscle cells by active mitogen-activated protein kinase kinase. *Mol. Biol. Cell.*, **6**, 1479–1490.
53. Liao, P., Wang, S.Q., Wang, S., Zheng, M., Zheng, M., Zhang, S.J., Cheng, H., Wang, Y. and Xiao, R.P. (2002) p38 mitogen-activated protein kinase mediates a negative inotropic effect in cardiac myocytes. *Circ. Res.*, **90**, 190–196.
54. Menick, D.R., Xu, L., Kappler, C., Jiang, W., Withers, P., Shepherd, N., Conway, S.J. and Muller, J.G. (2002) Pathways regulating Na+/Ca2+ exchanger expression in the heart. *Ann. N.Y. Acad. Sci.*, **976**, 237–247.
55. English, J.M. and Cobb, M.H. (2002) Pharmacological inhibitors of MAPK pathways. *Trends Pharmacol. Sci*, **23**, 40–45.
56. Bogoyevitch, M.A., Boehm, I., Oakley, A., Ketterman, A.J. and Barr, R.K. (2004) Targeting the JNK MAPK cascade for inhibition: basic science and therapeutic potential. *Biochim. Biophys. Acta*, **1697**, 89–101.
57. Lee, H.K., Braynen, W., Keshav, K., and Pavlidis, P. (2005) ErmineJ: tool for functional analysis of gene expression data sets. *BMC Bioinformatics*, **6**, 269.

FEBS Letters 582 (2008) 1189–1196

Affixin activates Rac1 via βPIX in C2C12 myoblast

Chie Matsuda[a,b,*], Kimihiko Kameyama[a], Atsushi Suzuki[c], Wataru Mishima[d], Satoshi Yamaji[d], Harumasa Okamoto[a], Ichizo Nishino[b], Yukiko K. Hayashi[b]

[a] *Neuroscience Research Institute, AIST, Central 6, 1-1-1 Higashi, Tsukuba, Ibaraki 305-8566, Japan*
[b] *Department of Neuromuscular Research, National Institute of Neuroscience, NCNP, Ogawa-Higashi, Kodaira, Tokyo 187-8502, Japan*
[c] *Department of Molecular Biology, Yokohama City University, Graduate School of Medicine, 3-9 Fukuura, Kanazawa-ku, Yokohama 236-0004, Japan*
[d] *Department of Internal Medicine and Clinical Immunology, Yokohama City University, Graduate School of Medicine, 3-9 Fukuura, Kanazawa-ku, Yokohama 236-0004, Japan*

Received 25 December 2007; accepted 31 January 2008

Available online 4 March 2008

Edited by Berend Wieringa

Abstract Affixin/β-parvin is an integrin-linked kinase (ILK)-binding focal adhesion protein highly expressed in skeletal muscle and heart. To elucidate the possible role of affixin in skeletal muscle, we established stable C2C12 cell line expressing T7-tagged human affixin (C2C12-affixin cells). Exogenous expression of affixin promotes lamellipodium formation where affixin, ILK αp21-activated kinase (PAK)-interactive exchange factor (PIX) and βPIX accumulate. The association of affixin and βPIX was confirmed by immunoprecipitation and pull down assay. In C2C12-affixin cells, an increased level of activated Rac1 but not Cdc42 was observed, and mutant βPIX lacking guanine nucleotide exchange factor activity inhibited lamellipodium formation. These results suggest that affixin is involved in reorganization of subsarcolemmal cytoskeletal actin by activation of Rac1 through α and βPIXs in skeletal muscle.

Structured summary:
MINT-6179203, MINT-6179212, MINT-6178859, MINT-6178812, MINT-6178832, MINT-6178843:
Affixin (uniprotkb:Q9HBI1) *physically interacts* (MI:0218) with *βpix* (uniprotkb:Q9ES28) by *coimmunoprecipitation* (MI:0019)
MINT-6179221:
Affixin (uniprotkb:Q9HBI1) *physically interacts* (MI:0218) with *αpix* (uniprotkb:Q8K4I3) by *coimmunoprecipitation* (MI:0019)
MINT-6178962, MINT-6178983:
Affixin (uniprotkb:Q9HBI1) *physically interacts* (MI:0218) with *βpix* (uniprotkb:Q9ES28) by *pull-down* (MI:0096)
MINT-6179002, MINT-6179021:
Affixin (uniprotkb:Q9HBI1) *binds* (MI:0407) *βpix* (uniprotkb:Q9ES28) by *pull-down* (MI:0096)
MINT-6179039:
PAK1 (uniprotkb:Q13153) *physically interacts* (MI:0218) with *Rac1* (uniprotkb:P63001) by *pull-down* (MI:0096)
MINT-6179054:
PAK1 (uniprotkb:Q13153) *physically interacts* (MI:0218) with *Cdc42* (uniprotkb:P70766) by *pull-down* (MI:0096)
MINT-6178790:
Affixin (uniprotkb:Q9HBI1) and *αpix* (uniprotkb:Q8K4I3) *colocalize* (MI:0403) by *fluorescence microscopy* (MI:0416)
MINT-6178760:
Affixin (uniprotkb:Q9HBI1) and *βpix* (uniprotkb:Q9ES28) *colocalize* (MI:0403) by *fluorescence microscopy* (MI:0416)
MINT-6178801:
Affixin (uniprotkb:Q9HBI1) and *dysferlin* (uniprotkb:Q9ESD7) *colocalize* (MI:0403) by *fluorescence microscopy* (MI:0416)
MINT-6178779:
Affixin (uniprotkb:Q9HBI1) and *ILK* (uniprotkb:O55222) *colocalize* (MI:0403) by *fluorescence microscopy* (MI:0416)

Keywords: Affixin/β-parvin; Lamellipodia; βPIX; Cytoskeletal actin

1. Introduction

Affixin/β-parvin (affixin) [1,2] is one of family of parvin family together with α-parvin/actopaxin/CH-ILKBP [1,3,4], and γ-parvin [1]. Parvins contain two caponin-homology (CH) domains and are known to have important role in focal adhesion, cell spreading and motility [5]. Our previous results revealed that affixin associates with αp21-activated kinase (PAK)-interactive exchange factor (PIX)/ARHGEF6/Cool-2 (αPIX) at the tips of lamellipodia of motile cells and transmits integrin-ILK signals which activate Cdc42 and Rac1, small Rho GTPases [6]. We also showed affixin directly binds to α-actinin which has a crucial role in reorganization of cytoskeletal actin [7]. Affixin is a protein highly expressed in skeletal muscle, and mainly localizes at sarcolemma [2]. We previously reported reduced sarcolemmal staining of affixin in dysferlin deficient skeletal muscles, and confirmed the association between affixin and dysferlin by an immunoprecipitation study [8]. Dysferlin is a sarcolemmal protein and its deficiency causes Miyoshi myopathy and limb girdle muscular dystrophy type 2B [9,10]. Based on the observation of

*Corresponding author. Fax: +81 29 861 6482.
E-mail address: c-matsuda@aist.go.jp (C. Matsuda).

Abbreviations: ILK, integrin-linked kinase; PIX, PAK-interactive exchange factor; C2C12-affixin, stable C2C12 cell line expressing T7-tagged human affixin; GEF, guanine nucleotide exchange factor; GST, gulutathione S-transferase; CH, caponin-homology; DH, Dbl-homology; PH, pleckstrin-homology; PAK, p21-activated kinase; CHO, Chinese hamster ovary

0014-5793/$34.00 © 2008 Federation of European Biochemical Societies. Published by Elsevier B.V. All rights reserved.
doi:10.1016/j.febslet.2008.01.064

dysferlin accumulation at wounded sarcolemmal sites, dysferlin is suggested to have an important role in Ca^{2+}-induced membrane repair [11]. These results imply participation of affixin in membrane repair process of skeletal muscle together with dysferlin, although the precise biological function of affixin in skeletal muscle is not yet clear.

In this study, we established stable C2C12 myoblast cell lines expressing human affixin (C2C12-affixin cells) to elucidate the possible role of affixin in skeletal muscle. The C2C12 myoblast is derived from mouse satellite cell and widely used as an in vitro model for skeletal muscle [12]. Here we show that exogenous overexpression of affixin promotes lamellipodium formation. In the C2C12-affixin cells, affixin is co-localized with βPIX/ARHGEF7/Cool-1 (βPIX) at lamellipodia together with αPIX, ILK and dysferlin. βPIX is a close homolog of αPIX and known to induce membrane ruffling [13]. The interaction of affixin with βPIX is confirmed by immunoprecipitation and pulldown assay. The level of activated Rac1 increased in the C2C12-affixin cells compared to C2C12 cells. Lamellipodium formation of the C2C12-affixin cells is suppressed by transfection of mutant αPIX or βPIX lacking guanine nucleotide exchange factor (GEF) activity. These results suggest an important role of affixin in subsarcolemmal actin reorganization by activation of Rac1 through α and βPIXs in skeletal muscle.

2. Materials and methods

2.1. Cell culture and establishment of stable transfectant

C2C12 myoblasts and COS-7 cells were maintained at 37 °C in a humidified atmosphere of 5% CO_2 in Dulbecco's modified Eagle's medium (Sigma) supplemented with 10% fetal bovine serum. C2C12 cells were transfected with T7-tagged human affixin cDNA subcloned into pcDNA3.1 (Invitrogen) using Lipofectamine 2000 (Invitrogen). All construct sequences were verified with DNA sequencing using ABI PRISM 310 (Applied Biosystems). The cells expressing T7-tagged human affixin were selected in growth media with 1 mg/ml G418 (Invitrogen). The surviving colonies were isolated and separately amplified. Cell line maintenance was performed with 0.5 mg/ml G418.

2.2. Antibodies

Monoclonal antibody against human dysferlin (NCL-Hamlet-2) was purchased from Novocastra. Rabbit polyclonal antibody against human affixin was previously characterized [2]. Rabbit polyclonal antibody against human αPIX was generated as described previously by Manser et al. [13]. We confirmed that affinity-purified anti-αPIX antibody did not cross-react with human βPIX expressed in COS-7 cells. Anti-ILK monoclonal antibody (Upstate Biotechnology), anti-βPIX polyclonal antibody (Chemicon International), anti-βPIX monoclonal antibody (BD Transduction Laboratories), anti-T7 polyclonal antibody (Omni-probe; Santa Cruz), anti-T7 monoclonal antibody (Novagen), anti-HA rat monoclonal antibody (3F10; Roche), anti-HA monoclonal antibody (262K; New England Biolabs), anti-$(His)_6$ polyclonal antibody (His-probe; Santa Cruz), anti-Rac1 (23A8; Upstate) and Cdc42 (clone 44; BD Transduction Laboratories) were used.

2.3. Immunofluorescent analysis

C2C12-affixin cells seeded on coverslips were fixed for 15 min in 2% paraformaldehyde in PBS and then permeabilized for 10 min in 0.1% Triton X-100 in PBS. For double immunolabeling with anti-affixin and anti-dysferlin antibodies, cells were fixed at −20 °C for 10 min in 100% methanol. Coverslips were blocked with 5% goat serum–2% BSA in PBS and then incubated with primary antibodies for double labelling. Immunolabeling was detected with goat anti-rabbit IgG conjugated to FITC and goat anti-mouse IgG conjugated to Cy3 antibodies (Jackson Immunoresearch Laboratories). Cells were observed with a confocal laser-scanning microscope (LSM5 PASCAL, Carl Zeiss).

2.4. Immunoprecipitation assay

C2C12 and C2C12-affixin cells were lysed in 50 mM Tris–HCl, pH 7.5, 150 mM NaCl, 1 mM EDTA, 1% NP-40 and Complete (Roche). The lysates precleared with Protein A/G-agarose (ImmunoPure, PIERCE) were incubated with anti-affixin, αPIX and βPIX polyclonal antibodies and then Protein A/G-agarose was added before an additional incubation. Immunoprecipitated proteins were dissociated from beads by boiling in sample buffer and resolved by SDS–PAGE. Immunoblotting was performed as previously described [14].

COS-7 cells were co-transfected with T7-tagged wild type or deletion mutant human affixin (RP1 and RP2) and HA-tagged human βPIX using FuGENE 6 (Roche), and lysed for immunoprecipitation after 48 h. Affixin deletion mutants were generated as previously described [2,6]. Human βPIX cDNA was cloned from KIAA0142 gifted by Dr. T. Nagase (Kazusa DNA Research Institute, Japan). Immunoprecipitation was performed as outlined above except that anti-T7 (Novagen) and anti-HA (New England BioLabs) antibodies were used.

2.5. Glutathione S-transferase (GST)-βPIX pulldown assay

The GST-βPIX proteins used for the pulldown assay were as follows: GST-SH3 (corresponding to amino acids of human βPIX 6-65), GST-Dbl-homology (DH) (aa 93–273), GST-pleckstrin-homology (PH) (aa 295–400), GST-CC (aa 586–638). cDNA fragments of these domains were amplified by PCR and subcloned into pGEX-5X-3 (GE Healthcare). GST fusion proteins expressed in BL21 were purified and bound to glutathione Sepharose 4B (GE Healthcare). The COS-7 cells overexpressing T7-tagged human affixin were lysed in the same lysis buffer used for immunoprecipitation. Precleared lysates were diluted with Buffer A (10 mM Tris–HCl, pH 8.0 and 0.1% Tween20) [15] and incubated with fusion protein bound to glutathione Sepharose 4B. After five washes in PBS, sample buffer was added to the beads and boiled for 5 min. Bound proteins were resolved by SDS–PAGE and subjected to immunoblotting using anti-T7 polyclonal antibody.

2.6. $(His)_6$-tagged affixin pulldown assay

cDNAs of deletion mutant affixin (RP1 and RP2) were amplified by PCR and subcloned into pET32a (Novagen). The $(His)_6$-tagged RP1 and RP2 were expressed in BL21DE3pLys(S), purified using Ni-NTA Spin kit (QIAGEN) and dialyzed against PBS. The pulldown assay using GST-βPIX fusion proteins and $(His)_6$-tagged RP1 or RP2 was performed as above.

2.7. Small GTPase activation assay

C2C12 and C2C12-affixin cells were grown until 60–70% confluence. Cells were lysed in 25 mM HEPES, pH 7.5, 150 mM NaCl, 1% Igepal CA-630, 10 mM $MgCl_2$, 1 mM EDTA and 2% glycerol. Lysates were incubated with glutathione Sepharose 4B conjugated with GST-p21-binding (CRIB) domain (residues 67–150) of human PAK-1 [16]. After three washes in the lysis buffer, the beads were resuspended in sample buffer and boiled for five minutes. Bound Rac1 and Cdc42 were separated on SDS–PAGE and subjected to immunoblotting.

2.8. Introduction of dominant-negative PIX into C2C12-affixin cells

Double mutation of βPIX (L238R, L239S) was introduced by PCR using appropriate internal primers. These two leucine residues were highly conserved among Dbl family member and shown to be essential for GEF activity [17]. βPIX and mutant βPIX (L238R, L239S) were subcloned into pSRD4-HA for transient expression. The constructs for transient expression of wild type αPIX and dominant negative αPIX (L383R, L384S) were as previously described [6]. C2C12-affixin cells were transfected with wild type or mutant PIX using Lipofectamine 2000. After 48 h, cells were fixed and immunolabeled as above.

3. Results

3.1. Immunofluorescent analysis of the C2C12-affixin cells

To investigate the possible role of affixin in skeletal muscle, stable C2C12 cell lines constitutively expressing T7-tagged human affixin were established. Expression of T7-tagged human affixin in C2C12-affixin cells was confirmed by immunoblot using anti-T7 antibody (Fig. 2). The expression level of total

affixin of C2C12-affixin cells was slightly higher than original C2C12 cell on immunoblotting using anti-affixin antibody (data not shown). Exogenous expression of T7-affixin in the C2C12 cells induced lamellipodia (Fig. 1). Only 10–20% of original C2C12 myoblasts showed lamellipodium formation, while more than half of the C2C12-affixin cells formed lamellipodia without any stimulation (Fig. 1). Formation of lamellipodia was confirmed by labelling F-actin with rhodamine–phalloidin.

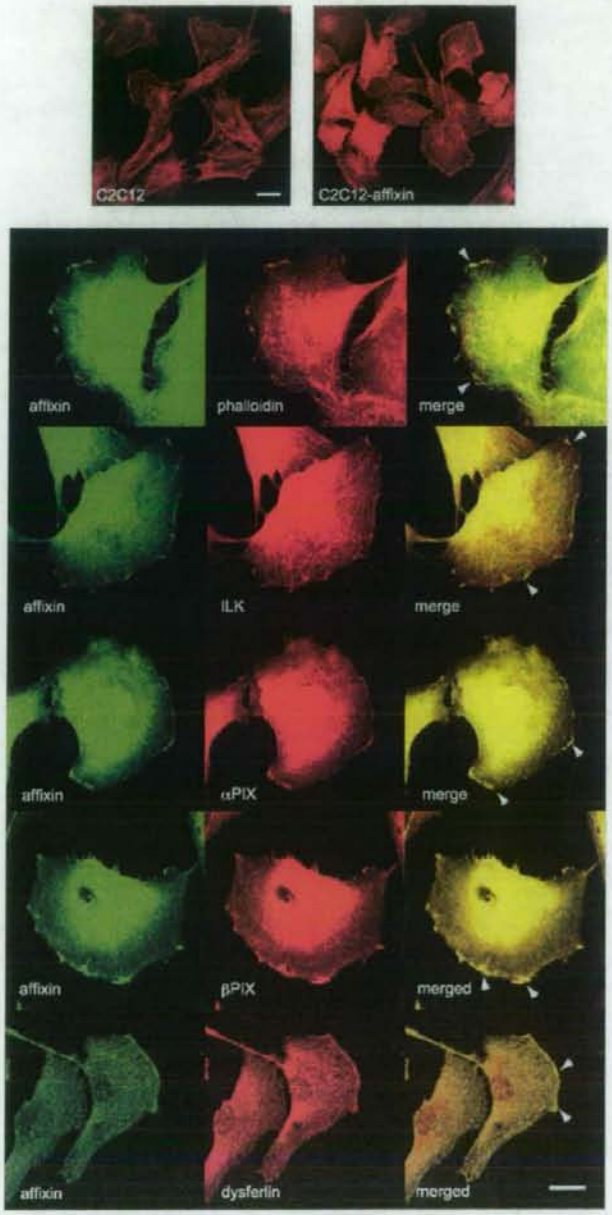

Fig. 1. Immunofluorescence analysis of stable C2C12 cells expressing human affixin. Lamellipodium formation was confirmed by rhodamine-phalloidin labelling. Antibodies were applied in five double-staining combinations: anti-affixin and phalloidin; anti-affixin and ILK; anti-T7 and αPIX; anti-affixin and βPIX and anti-affixin and dysferlin. Exogenous affixin was labelled with anti-T7 monoclonal antibody. Affixin co-localizes with ILK, αPIX, βPIX and dysferlin lamellipodium tips (arrowheads) in the C2C12-affixin cells. Scale bar, 20 μm.

As shown in Fig. 1, affixin accumulated and co-localized with F-actin at the tips of lamellipodia (Fig. 1). Transient expression of affixin without T7-tag promoted the lamellipodium formation of C2C12 cells as T7-tagged affixin (data not shown). Exogenous affixin was expressed in both the cytoplasm and at the tips of lamellipodia as C2C12-endogenous affixin (data not shown). We have previously shown the co-localization of affixin and ILK, a binding partner of affixin, at focal adhesion and at the tips of leading edge in Chinese hamster ovary (CHO) cells [2], and at sarcolemma of human skeletal muscle fibers [8]. In C2C12-affixin cells, ILK was enriched and co-localized with affixin in lamellipodia (Fig. 1) as original C2C12 cells. Cytoplasmic affixin in the C2C12-affixin cells was partially co-localized with ILK.

αPIX, a binding partner of affixin co-localizes with exogenous affixin at the tips of lamellipodia in 3Y1 cells (rat fibroblasts) [6] and CHO-K1 cells [18]. In the C2C12-affixin cells, endogenous αPIX accumulated intensely at the tips lamellipodia and co-localized with affixin (Fig. 1), while diffuse fine cytoplasmic granular staining of αPIX without lammellipodium accumulation was observed in the original C2C12 cells (data not shown). The C2C12-affixin cells also showed intense staining of βPIX, a homolog and a binding partner of αPIX [18,19], at lamellipodia, suggesting a possible association of affixin and βPIX. The co-localization of βPIX and affixin was observed at lamellipodia of original C2C12 cells (data not shown). Cytoplasmic α and βPIXs were also co-localized with affixin in the C2C12 cells. We then examined subcellular localization of dysferlin, a binding partner of affixin, in C2C12-affixin cells. As we reported earlier, cytoplasmic granular staining of dysferlin with no sarcolemmal accumulation was observed in the undifferentiated C2C12 cells [8]. In the C2C12-affixin cells, dysferlin accumulated and co-localized with affixin at lamellipodia. These results show that affixin co-localizes with ILK, αPIX, βPIX and dysferlin at the tips lamellipodia in the C2C12-affixin cells.

3.2. Analysis of the association between affixin and βPIX by coimmunoprecipitation assay

To define possible association between affixin and βPIX, immunoprecipitation was performed using the C2C12-affixin and original C2C12 cells. As shown in Fig. 2A, affixin was specifically co-immunoprecipitated with anti-βPIX antibody and reciprocally, βPIX was specifically co-immunoprecipitated by anti-affixin antibody in both C2C12-affixin and original C2C12 cells. There is no significant quantitative difference in co-immunoprecipitated affixin, α and βPIXs between C2C12-affixin and original C2C12 cells. Further, αPIX was specifically co-immunoprecipitated by anti-affixin [6] and anti-βPIX [18,19] antibodies in C2C12-affixin and original C2C12 cells as previously reported. Affixin or βPIX was not co-immunoprecipitated by control rabbit IgG.

To identify the region within affixin that interacts with βPIX, immunoprecipitation was also performed using COS-7 cells transiently co-transfected with full-length or deletion mutants [2] of T7-human affixin (Fig. 2A) and HA-human βPIX. As shown in Fig. 2B, the full-length T7-affixin was co-immunoprecipitated by anti-HA antibody. Reciprocally, HA-βPIX was specifically co-immunoprecipitated by anti-T7 antibody, while control mouse IgG was not. Affixin-RP1 containing N-terminal CH domain (CH1) was co-immunoprecipitated by

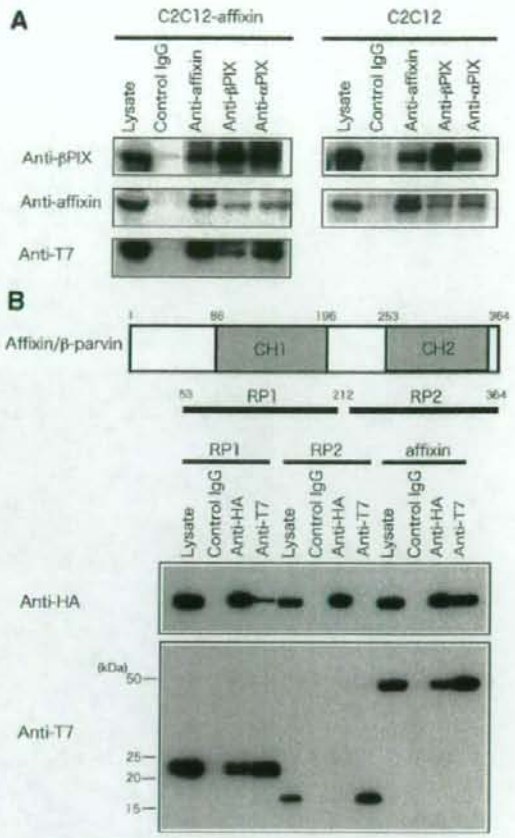

Fig. 2. (A) Confirmation of the association of affixin and βPIX. Cell lysates form the C2C12-affixin and C2C12 cells were immunoprecipitated with anti-affixin, anti-βPIX and anti-αPIX antibodies. Immunoprecipitates were subjected to immunoblotting with the same antibodies used for immunoprecipitation. Affixin was specifically co-immunoprecipitated by anti-βPIX antibody and *vice versa*. Co-immunoprecipitation of T7-tagged exogenous affixin was confirmed by probing with anti-T7 antibody. As reported previously, αPIX was specifically co-immunoprecipitated by anti-affixin and anti-βPIX antibodies. (B) Identification of βPIX-binding domain of affixin by immunoprecipitation assay. T7-tagged wild type or deletion mutants of affixin and HA-tagged βPIX were co-expressed in COS-7 cells. A schema of deletion mutants of affxin is shown at the top. Immunoprecipitation was performed with anti-T7 and anti-HA antibodies. βPIX was co-immunoprecipitated with wild type affixin and RP1 and *vice versa*, but not with RP2.

HA-βPIX (Fig. 2B), while affixin-RP2 containing C-terminal CH domain (CH2) was not. These and previous reported findings [6] suggest that affixin can interact with both α and βPIXs via CH1 domain.

3.3. Identification of the binding domain of βPIX to affixin by pulldown assay

To identify affixin-binding domain of βPIX, a pulldown assay was performed. The lysates from COS-7 cells overexpress-

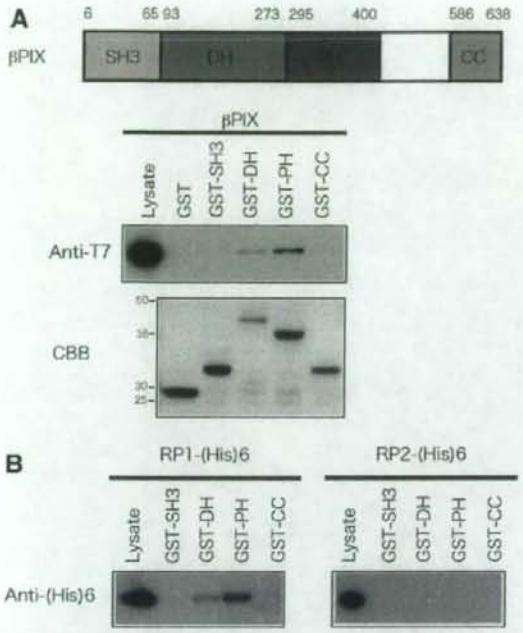

Fig. 3. Identification of affixin-binding domain in βPIX by pulldown assay. (A) Cell lysates from COS-7 cells overexpressing T7-tagged affixin were incubated with glutathione Sepharose 4B beads bound to GST, GST-SH3, GST-DH, GST-PH and GST-CC. Domain structures of βPIX are shown at the top. After overnight incubation at 4 °C, the beads were washed and bound proteins were subjected to immunoblotting with anti-T7 polyclonal antibody. A band at 50 kDa, which corresponds to T7-affixin, was detected in GST-DH and GST-PH. GST fusion proteins used for the pulldown assay were stained with coomasie brilliant blue. GST, GST-SH3, GST-DH, GST-PH and GST-CC domains have molecular masses of 26, 32.8, 46.6, 38 and 32.3 kDa, respectively. (B) Bacterially expressed $(His)_6$-tagged RP1 and RP2 were purified and incubated with GST-βPIX domains as described above. The proteins bound to GST fusion proteins were subjected to immunoblotting using anti-$(His)_6$ antibody.

ing T7-affixin were incubated with GST fusion proteins carrying each domain of human βPIX bound to glutathione Sepharose 4B. Fig. 3A shows that the DH and PH domains of βPIX can interact with T7-affixin, whereas the SH3 and CC domains of βPIX failed. PH domain of βPIX showed higher affinity to T7-affixin than DH domain of βPIX. To examine whether affixin-RP1 directly binds to DH and PH domains of βPIX, pulldown assay was performed using bacterially expressed $(His)_6$-tagged RP1 instead of cell lysate. As shown in Fig. 3B, $(His)_6$-tagged RP1 was bound to DH and PH domains of βPIX, whereas $(His)_6$-tagged RP2 failed to interact with any domain of βPIX. PH domain of βPIX showed higher affinity to $(His)_6$-tagged RP1 than DH domain of βPIX. These results were consistent with the result of a pulldown assay using cell lysates and suggest direct interaction between affixin and βPIX.

3.4. Rac1 but not Cdc42 is activated in C2C12-affixin cells

The reorganization of cytoskeletal actin is regulated by Rho family small GTPases. βPIX is known as a specific GEF for

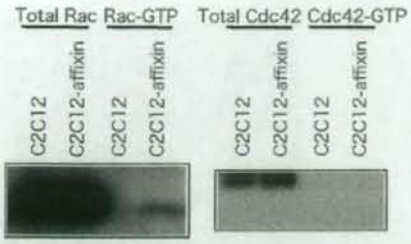

Fig. 4. Pulldown assay of active Rac1 and Cdc42. C2C12-affixin and C2C12 cells were lysed and incubated with glutathione Sepharose 4B conjugated with GST-p21-binding (CRIB) domain (residues 67–150) of human PAK-1. The CRIB domain specifically associates with Rac-GTP and Cdc42-GTP. The total amounts of Rac1 and Cdc42 were assessed by the immunoblotting using the cell lysates.

Rac1/Cdc42 and induces membrane ruffling [13]. To examine whether Rac1/Cdc42 is activated in the C2C12-affixin cells, a pulldown assay was performed using GST-fusion protein derived from PAK, the effector protein of Rac1 and Cdc42. Cell lysates from C2C12-affixin and C2C12 cells were incubated with GST-p21 binding domain of PAK bound to glutathione Sepharose 4B. This analysis revealed increased level of Rac1-GTP in the C2C12-affixin cells (Fig. 4). There was no significant difference in Cdc42-GTP. The total expression levels of Rac1 and Cdc42 protein in the C2C12-affixin were equivalent to the C2C12 cells. These results indicate that the exogenous expression of affixin can activate Rac1 but not Cdc42 in C2C12 cells.

3.5. Dominant-negative βPIX suppresses lamellipodium formation in the C2C12-affixin cells

Activation of Rac1 is mediated by GEFs including βPIX [20]. To examine the involvement of βPIX in lamellipodium formation observed in the C2C12-affixin cells, the HA-tagged dominant negative mutant of βPIX were introduced into the C2C12-affixin cells. Exogenous βPIX and affixin were labelled with anti-HA and anti-T7 antibodies, respectively. As shown in Fig. 5, the C2C12-affixin cells overexpressing wild type βPIX form lamellipodia as observed in the C2C12-affixin cells without transfection. In contrast, dominant negative mutant of βPIX (L238R, L239S) suppressed the lamellipodium formation in the C2C12-affixin cells. The association of dominant negative βPIX and affixin was confirmed by an immunoprecipitation study using COS-7 cells (data not shown). Similar inhibition of lamellipodium formation was observed in the C2C12-affixin cells transfected with dominant negative mutant of αPIX. In C2C12-affixin cells transiently transfected with dominant negative mutants of PIX, expression level of affixin, α and βPIXs was equivalent to C2C12-affixin cells without transfection on immunoblot (data not shown). These results suggest that both α and βPIXs are necessary for the lamellipodium formation in the C2C12-affixin cells.

4. Discussion

Lamellipodium is the dynamic actin-based structure and its formation is mediated by the activation of Rho family small GTPases and their effector proteins. Small Rho GTPases are activated by GEFs, which catalyze exchange of GDP for

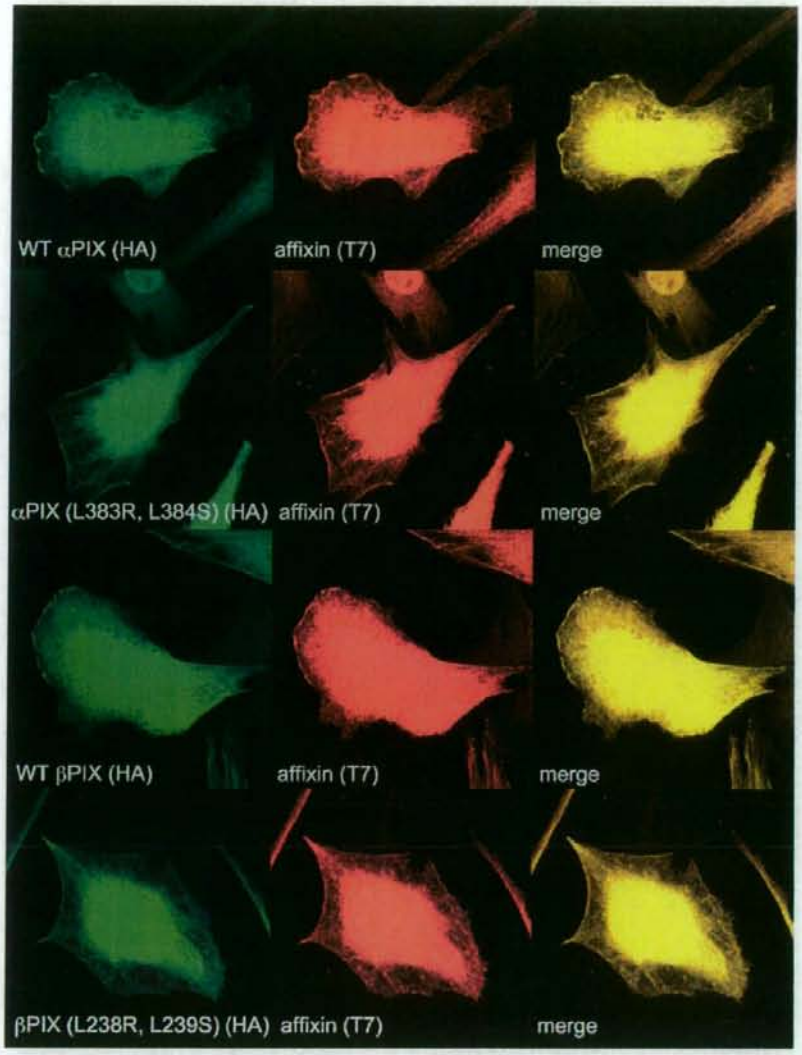

Fig. 5. Immunofluorescence analysis of the C2C12-affixin cells transformed with the dominant negative mutants of PIXs. The C2C12-affixin cells were transfected with wild type or dominant negative mutants of PIXs, αPIX (L383R, L384S) and βPIX (L238R, L239S). Exogenous PIX and affixin were simultaneously immunolabeled with anti-HA and anti-T7 antibodies, respectively. Scale bar, 20 μm.

GTP. GEFs are regulated by protein–protein interaction, oligomerization and relief of intramolecular inhibitory sequence [21]. More than 60 GEFs including PIXs have been identified in human genomic sequences [22]. βPIX expression levels are highest in skeletal muscle by Northern blot analysis using KIAA clones as probes (KIAA0142, http://www.kazusa.or.jp/huge/gfimage/northern/html/KIAA0142.html).

In C2C12 cells, exogenous expression of affixin induced prominent lamellipodia. Accumulated βPIX, together with ILK was observed at the tips of lammelipodia and co-localized with affixin. The interaction of affixin and βPIX was confirmed by immmunoprecipitation and pulldown assays. These data suggest that affixin could promote reorganization of subsarcolemmal actin cytoskeleton associated with accumulation of GEFs.

We previously demonstrated that Madin-Darby canine kidney cells overexpressing CH1 domain of affixin formed membrane protrusions, while control cells transfected with lacZ showed a cobble-like morphology [6]. This CH1-induced reorganization of cytoskeletal actin is mediated by the activation of both Rac1 and Cdc42 through αPIX. Interestingly, only Rac1 but not Cdc42 is activated in the C2C12-affixin cells used for this study. αPIX has been reported to contain Rac-specific interaction domain at C-terminus of PH domain [23]. When

αPIXs form a homodimer, the DH domain of one molecule and Rac-specific interaction domain of another molecule work together and bind Rac specifically, whereas monomeric αPIX can interact with Cdc42 as well as Rac. Despite the lack of a Rac-specific interaction domain, βPIX binds directly and activates Rac1 specifically but not Cdc42 in human embryonal kidney 293 cells [24]. Previous study using yeast two hybrid system [18,19] and our immunoprecipitation results have shown that α and βPIX form heterodimers in the C2C12-affixin cells (Fig. 2A), although their specificity for small GTPase remains unclear. We have also shown that lamellipodium formation in the C2C12-affixin cells was inhibited by overexpression of dominant negative forms of α or βPIX (Fig. 5). From these results, we suspect that the DH domain of βPIX and the Rac-specific interacting domain of αPIX work together and activate specifically Rac1. Further analyses are needed to elucidate the precise regulation of GEF activity of both PIXs in C2C12-affixin cells.

Lamellipodium formation is essential for cell motility. In epithelial cell monolayer, the cells around the wounded edge form lamellipodia and activation of Rac1 but not Cdc42 or Rho is required for wound closure [25]. Similarly, activated satellite cells form lamellipodia and migrate around the injured lesion during skeletal muscle regeneration [26]. Very recently, dysferlin reportedly localized in the T-tubule system of differentiating C2C12 cells and was recruited to the wounded site [27]. Dysferlin is known to have an important role in skeletal muscle wound healing [11]. In response to the sarcolemmal injury of muscle fibers, dysferlin patch was formed around wounded sites for resealing in a calcium-dependent manner. Calcium-dependent membrane resealing is also reported in wounded *Xenopus* oocyte, where Cdc42 and RhoA are activated [28]. Membrane repair is composed of two process: plasma membrane resealing and reorganization of subsarcolemmal cytoskeleton [29]. Accumulation of dysferlin and activation of Rac1 via PIXs in the lamellipodia of C2C12-affixin cells may suggest the involvement of these molecules in sarcolemmal repair followed by cytoskeletal actin reorganization.

In conclusion, exogenous expression of affixin promotes lamellipodium formation in C2C12 myoblasts via activation of Rac1 by α and βPIXs. Reorganization of cytoskeletal actin mediated by affixin may be involved in the skeletal muscle dysferlin-related membrane repair system.

Acknowledgements: This work was supported by Grants-in-aid for Scientific Research (C.M.; C, 15590924, 18590966) (Y.K.H.; B, 18390265), and Grant-in-Aid for Exploratory Research (Y.K.H.; 50238135) from the Japan Society for the Promotion of Science, the Nakatomi Foundation (C.M.), the Research on Psychiatric and Neurological Diseases and Mental Health from Health and Labor Sciences Research Grants (Y.K.H. and I.N.), and the Research Grant for Nervous and Mental Disorders, from the Ministry of Health, Labour and Welfare (I.N.).

References

[1] Olski, T.M., Noegel, A.A. and Korenbaum, E. (2001) Parvin, a 42 kDa focal adhesion protein, related to the alpha-actinin superfamily. J. Cell Sci. 114, 525–538.
[2] Yamaji, S. et al. (2001) A novel integrin-linked kinase-binding protein, affixin, is involved in the early stage of cell-substrate interaction. J. Cell Biol. 153, 1251–1264.
[3] Nikolopoulos, S.N. and Turner, C.E. (2000) Actopaxin, a new focal adhesion protein that binds paxillin LD motifs and actin and regulates cell adhesion. J. Cell Biol. 151, 1435–1448.
[4] Tu, Y., Huang, Y., Zhang, Y., Hua, Y. and Wu, C. (2001) A new focal adhesion protein that interacts with integrin-linked kinase and regulates cell adhesion and spreading. J. Cell Biol. 153, 585–598.
[5] Sepulveda, J.L. and Wu, C. (2006) The parvins. Cell. Mol. Life Sci. 63, 25–35.
[6] Mishima, W. et al. (2004) The first CH domain of affixin activates Cdc42 and Rac1 through alphaPIX, a Cdc42/Rac1-specific guanine nucleotide exchanging factor. Gene Cell 9, 193–204.
[7] Yamaji, S. et al. (2004) Affixin interacts with alpha-actinin and mediates integrin signaling for reorganization of F-actin induced by initial cell–substrate interaction. J. Cell Biol. 165, 539–551.
[8] Matsuda, C. et al. (2005) Dysferlin interacts with affixin (beta-parvin) at the sarcolemma. J. Neuropathol. Exp. Neurol. 64, 334–340.
[9] Liu, J. et al. (1998) Dysferlin, a novel skeletal muscle gene, is mutated in Miyoshi myopathy and limb girdle muscular dystrophy. Nat. Genet. 20, 31–36.
[10] Bashir, R. et al. (1998) A gene related to *Caenorhabditis elegans* spermatogenesis factor fer-1 is mutated in limb-girdle muscular dystrophy type 2B. Nat. Genet. 20, 37–42.
[11] Bansal, D., Miyake, K., Vogel, S.S., Groh, S., Chen, C.C., Williamson, R., McNeil, P.L. and Campbell, K.P. (2003) Defective membrane repair in dysferlin-deficient muscular dystrophy. Nature 423, 168–172.
[12] Yaffe, D. and Saxel, O. (1977) Serial passaging and differentiation of myogenic cells isolated from dystrophic mouse muscle. Nature 270, 725–727.
[13] Manser, E. et al. (1998) PAK kinases are directly coupled to the PIX family of nucleotide exchange factors. Mol. Cell 1, 183–192.
[14] Matsuda, C., Aoki, M., Hayashi, Y.K., Ho, M.F., Arahata, K. and Brown Jr., R.H. (1999) Dysferlin is a surface membrane-associated protein that is absent in Miyoshi myopathy. Neurology 53, 1119–1122.
[15] Sotgia, F. et al. (2000) Caveolin-3 directly interacts with the C-terminal tail of beta -dystroglycan. Identification of a central WW-like domain within caveolin family members. J. Biol. Chem. 275, 38048–38058.
[16] del Pozo, M.A., Price, L.S., Alderson, N.B., Ren, X.D. and Schwartz, M.A. (2000) Adhesion to the extracellular matrix regulates the coupling of the small GTPase Rac to its effector PAK. EMBO J. 19, 2008–2014.
[17] Hart, M.J., Eva, A., Zangrilli, D., Aaronson, S.A., Evans, T., Cerione, R.A. and Zheng, Y. (1994) Cellular transformation and guanine nucleotide exchange activity are catalyzed by a common domain on the dbl oncogene product. J. Biol. Chem. 269, 62–65.
[18] Rosenberger, G., Jantke, I., Gal, A. and Kutsche, K. (2003) Interaction of alphaPIX (ARHGEF6) with beta-parvin (PARVB) suggests an involvement of alphaPIX in integrin-mediated signaling. Hum. Mol. Genet. 12, 155–167.
[19] Koh, C.G., Manser, E., Zhao, Z.S., Ng, C.P. and Lim, L. (2001) Beta1PIX, the PAK-interacting exchange factor, requires localization via a coiled-coil region to promote microvillus-like structures and membrane ruffles. J. Cell Sci. 114, 4239–4251.
[20] Scita, G., Tenca, P., Frittoli, E., Tocchetti, A., Innocenti, M., Giardina, G. and Di Fiore, P.P. (2000) Signaling from Ras to Rac and beyond: not just a matter of GEFs. EMBO J. 19, 2393–2398.
[21] Schmidt, A. and Hall, A. (2002) Guanine nucleotide exchange factors for Rho GTPases: turning on the switch. Gene Dev. 16, 1587–1609.
[22] Venter, J.C. et al. (2001) The sequence of the human genome. Science 291, 1304–1351.
[23] Feng, Q., Baird, D. and Cerione, R.A. (2004) Novel regulatory mechanisms for the Dbl family guanine nucleotide exchange factor Cool-2/alpha-Pix. EMBO J. 23, 3492–3504.
[24] ten Klooster, J.P., Jaffer, Z.M., Chernoff, J. and Hordijk, P.L. (2006) Targeting and activation of Rac1 are mediated by the exchange factor beta-Pix. J. Cell Biol. 172, 759–769.

[25] Fenteany, G., Janmey, P.A. and Stossel, T.P. (2000) Signaling pathways and cell mechanics involved in wound closure by epithelial cell sheets. Curr. Biol. 10, 831–838.
[26] Bischoff, R. and Flanzini-Armstrong, C. (2004) Stellite and stem cells in muscle regeneration. Myology, 66–86.
[27] Klinge, L., Laval, S., Keers, S., Haldane, F., Straub, V., Barresi, R. and Bushby, K. (2007) From T-tubule to sarcolemma: damage-induced dysferlin translocation in early myogenesis. FASEB J.
[28] Benink, H.A. and Bement, W.M. (2005) Concentric zones of active RhoA and Cdc42 around single cell wounds. J. Cell Biol. 168, 429–439.
[29] Bement, W.M., Yu, H.Y., Burkel, B.M., Vaughan, E.M. and Clark, A.G. (2007) Rehabilitation and the single cell. Curr. Opin. Cell Biol. 19, 95–100.

Neuromuscular Disorders 18 (2008) 959–961

Contents lists available at ScienceDirect

Neuromuscular Disorders

journal homepage: www.elsevier.com/locate/nmd

Case report

Rigid spine syndrome caused by a novel mutation in four-and-a-half LIM domain 1 gene (*FHL1*)

Sherine Shalaby, Yukiko K. Hayashi*, Kanako Goto, Megumu Ogawa, Ikuya Nonaka, Satoru Noguchi, Ichizo Nishino

Department of Neuromuscular Research, National Institute of Neuroscience, National Center of Neurology and Psychiatry (NCNP), 4-1-1 Ogawahigashi-cho, Kodaira, Tokyo 187-8502, Japan

ARTICLE INFO

Article history:
Received 19 May 2008
Received in revised form 9 September 2008
Accepted 17 September 2008

Keywords:
Four-and-a-half LIM domain 1 (*FHL1*)
Rigid spine syndrome
Reducing body

ABSTRACT

Four-and-a-half LIM domain 1 gene (*FHL1*) has recently been identified as the causative gene for reducing body myopathy (RBM), X-linked scapuloperoneal myopathy (SPM) and X-linked myopathy with postural muscle atrophy (XMPMA). Rigid spine is a common clinical feature of the three diseases. We searched for *FHL1* mutations in eighteen patients clinically diagnosed as rigid spine syndrome (RSS). We identified one RSS patient with *FHL1* mutation. Reducing bodies were observed in few fibers of the patient's muscle sample. Amount of FHL1 protein was decreased on immunoblotting. In conclusion, *FHL1* can be one of the causative genes for RSS.

1. Introduction

FHL1, four-and-a-half LIM domain 1 is a 32 kDa protein which is highly expressed in skeletal muscle with intermediate expression in the heart [1]. LIM domains are a cysteine-rich double zinc finger protein-binding motif denoted by the sequence (CX2–CX17–19HX2C)X2(CX2CX16–20CX2(H/D/C)) and mediate interactions with transcription factors and cytoskeletal proteins. LIM domain proteins play critical roles in tissue differentiation and cytoskeletal integrity, respectively. FHL1 was implicated in many cellular functions; (1) α5β1-integrin-dependent myocyte elongation [2], (2) regulation of myosin filament formation and sarcomere assembly by binding to myosin-binding protein C [3], and (3) modulation of Notch signalling pathway through interaction of FHL1C (one of the splicing isoforms of FHL1) with transcription factor RBP-J and RING1 [4].

Recently, mutations in *FHL1* have been identified in patients with RBM [5], SPM [6] and XMPMA [7]. We have also identified mutations in *FHL1* in all RBM patients we reported previously, and confirmed that *FHL1* is the causative gene for RBM (unpublished data). Clinical picture of RBM patients varies from congenital lethal form to benign childhood and adult forms. However, four out of the six RBM families reported to date show rigid spine [5,8]. In addition rigid spine was reported in SPM families [9] and was also seen in the British and Italian–American families reported as XMPMA [7]. This finding suggests that rigid spine is a common clinical feature of patients with *FHL1* mutations.

Here we found a patient with rigid spine syndrome (RSS) harboring a mutation in *FHL1* among 18 patients clinically diagnosed as RSS.

2. Case report

The patient is a 16-year-old male who was a good runner during his childhood. He was first noted to have scoliosis on a routine medical examination when he was 13 years old. Gradually, his walking and running speed became slower, and hip muscle atrophy was noted. Two years late he started experiencing difficulty in bending his body and difficulty in neck flexion. He could not stand on one foot. By the age of 16 years, bilateral hip and thigh muscle atrophy was prominent. On examination, he showed muscle weakness and atrophy in the sternomastoid, trapezius, paravertebral, pelvic girdle and proximal lower limb muscles. Winging of scapula and Gowers' sign were observed. Funnel chest and joint contractures in neck, spine, hip and ankle joints were seen. He walked slouchingly and his left leg was slightly lagged and outward rotated. Serum creatine kinase level was mildly elevated and respiratory functions were mildly impaired. His elder brother showed mild scoliosis but not rigid spine or muscle weakness. His father had IRBBB while his mother was healthy.

Genomic DNA was isolated from peripheral lymphocytes using a standard technique after obtaining informed consent. Seven sets of primers were used to amplify genomic fragments of *FHL1*. All

* Corresponding author. Tel.: +81 42 346 1712; fax: +81 42 346 1742.
E-mail address: hayasi_y@ncnp.go.jp (Y.K. Hayashi).

0960-8966/$ - see front matter © 2008 Elsevier B.V. All rights reserved.
doi:10.1016/j.nmd.2008.09.012

exons and their flanking intronic regions of *FHL1* were directly sequenced using an ABI PRISM 3100 automated sequencer (PE Applied Biosystems). We identified a hemizygous in-frame nine base-pair (bp) deletion mutation at c.451–459delGTGACTTGC (p.151–153delVTC) of *FHL1* in this patient. A total 250 controls and the other 17 RSS patients did not carry the mutation in *FHL1*. Genetic analysis of other family members including the elder brother was not allowed.

Biopsied muscle specimen was frozen in isopentane cooled in liquid nitrogen. Serial 10 μm cryostat sections were stained with haematoxylin and eosin (HE), modified Gomori trichrome (mGt) and a battery of histochemical methods. Menadione–nitroblue tetrazolium (NBT) staining in the absence of the substrate α-glycerophosphate was also performed to detect reducing bodies (RBs). Histological analyses of muscle showed marked variation in fiber size and fibers with rimmed vacuoles. Only a limited number of fibers contained RBs. These abnormal fibers detected were localized in focal areas of the muscle specimen (Fig. 1A and B).

Immunohistochemical analysis revealed diffusely increased FHL1 staining in some muscle fibers. The strong FHL1 staining was observed in both types of fibers as seen in serial sections stained by slow type of myosin heavy chain (MHC-slow) (Fig. 1C and D). Protein amount of FHL1 by immunoblotting analysis was significantly reduced in the patient muscle when compared to normal control after normalization to actin amount (Fig. 2).

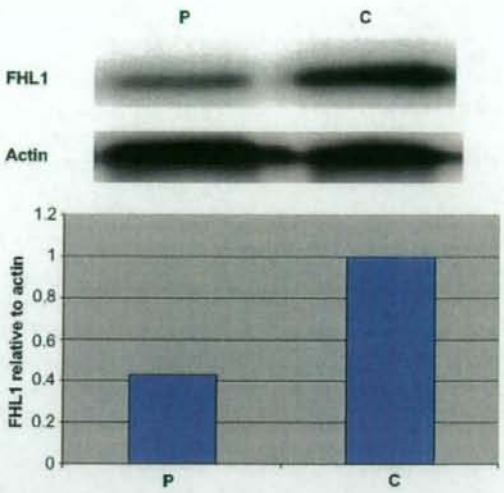

Fig. 2. Immunoblotting analysis of FHL1. Amount of FHL1 in biopsied muscle from the RSS patient show significant reduction compared to actin.

3. Discussion

The term *rigid spine syndrome* was first proposed by Dubowitz to highlight the essential clinical problem seen in myopathy with prominent spinal rigidity [10]. Nevertheless, spinal rigidity is not a specific finding as it is a characteristic feature in Emery–Dreifuss muscular dystrophy, Bethlem myopathy, and in selenoprotein related myopathies. In addition it has also been reported in other congenital myopathies and muscular dystrophies. Patients with *FHL1* mutations also show spinal rigidity [5,7,9].

Here we identified a RSS patient with a novel mutation in *FHL1*. The mutation affects a cysteine residue in the second LIM domain of FHL1 similar to all mutations causing RBM [5].

The most important feature to differentiate RSS from other muscular diseases associated with spinal rigidity is the limitation of flexion of the cervical and dorsolumbar spine in absence of

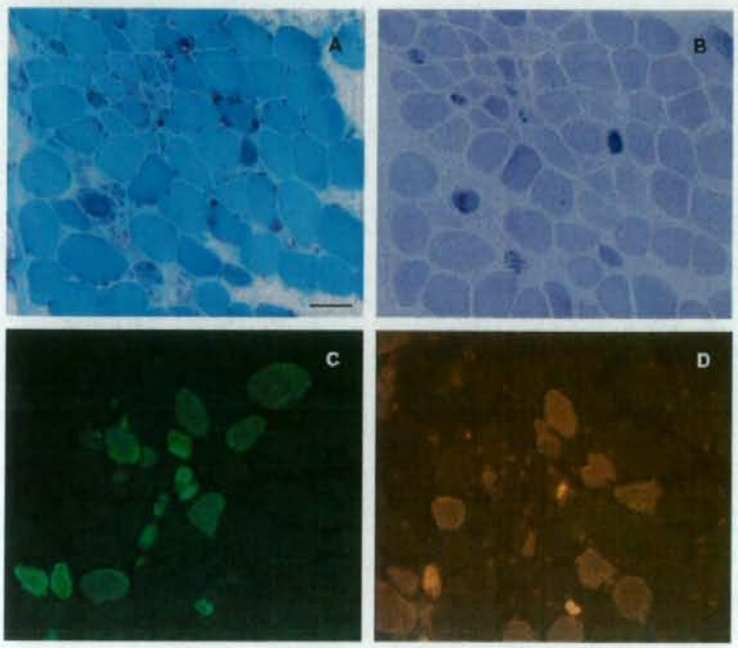

Fig. 1. Muscle pathology. (A) Intracytoplasmic inclusions and rimmed vacuoles are seen on mGT staining. (B) Reducing bodies are positive on melanodine–NBT staining. (C) Diffuse strong immunoreactivity to FHL1 is seen in both MyHC-slow positive and negative fibers (D). Bar = 20 μm.